A Project Report on

EXPLORING QUANTUM CONVOLUTIONAL NEURAL NETWORK FOR GRAVITATIONAL WAVE DETECTION WITH THERMAL NOISE ANALYSIS

Submitted in partial fulfillment of requirement for the award of

MASTER OF COMPUTER APPLICATIONS

OF

KANNUR UNIVERSITY

BY

VYSHNAV K P

IT22GMCAD17

SCHOOL OF INFORMATION SCIENCE AND TECHNOLOGY

Kannur University Campus

Mangattuparamba

Kannur – 670567

2022 - 2024

A Project Report on

EXPLORING QUANTUM CONVOLUTIONAL NEURAL NETWORK FOR GRAVITATIONAL WAVE DETECTION WITH THERMAL NOISE ANALYSIS

Submitted in partial fulfillment of requirement for the award of

MASTER OF COMPUTER APPLICATIONS

OF

KANNUR UNIVERSITY

BY

VYSHNAV K P

IT22GMCAD17

SCHOOL OF INFORMATION SCIENCE AND TECHNOLOGY

Kannur University Campus

Mangattuparamba

Kannur – 670567

2022 - 2024

DECLARATION

I Vyshnav K P , fourth semester MCA student, hereby declare that the project report entitled "**EXPLORING QUANTUM CONVOLUTIONAL NEURAL NETWORK FOR GRAVITATIONAL WAVE DETECTION WITH THERMAL NOISE ANALYSIS** "submitted in partial fulfillment of the requirement for the award ofthe MCA, is a report of the original work done by me during the period of study at School of Information Science and Technology, Mangattuparamba under the supervision of **Ms.Shylaja P , Internal Guide, Department of IT, School of Information Science and Technology, Kannur university**

Place: Mangattuparamba

Date:

VYSHNAV K P

IT22GMCAD17

KANNUR UNIVERSITY

SCHOOL OF INFORMATION SCIENCE AND TECHNOLOGY

KANNUR UNIVERSITY CAMPUS MANGATTUPARAMBA

KANNUR-670567

Certificate

This is to certify that the project entitled "EXPLORING QUANTUM CONVOLUTIONAL NEURAL NETWORK FOR GRAVITATIONAL WAVE DETECTION WITH THERMAL NOISE ANALYSIS" submitted in partial fulfillment of the requirement for the award of **Master of Computer Application** *Degree, is a result of bonafied work carried out by* **Mr. Vyshnav K P, IT22GMCAD17** *during the year 2022- 2024.*

Ms.Shylaja P
(Internal guide)

Dr. N. S Sreekanth
(Head of the Department)

Place: Mangattuparamba

Date:

External Examiners

1)

2)

Digital Receipt

This receipt acknowledges that Turnitin received your paper. Below you will find the receipt information regarding your submission.

The first page of your submissions is displayed below.

Submission author:	Ebin Antony
Assignment title:	PGDDSA
Submission title:	QCNN
File name:	REPORT-3_VYSHNAV_2.docx
File size:	6.4M
Page count:	74
Word count:	15,441
Character count:	92,696
Submission date:	22-Jun-2024 06:08PM (UTC+0530)
Submission ID:	2222570309

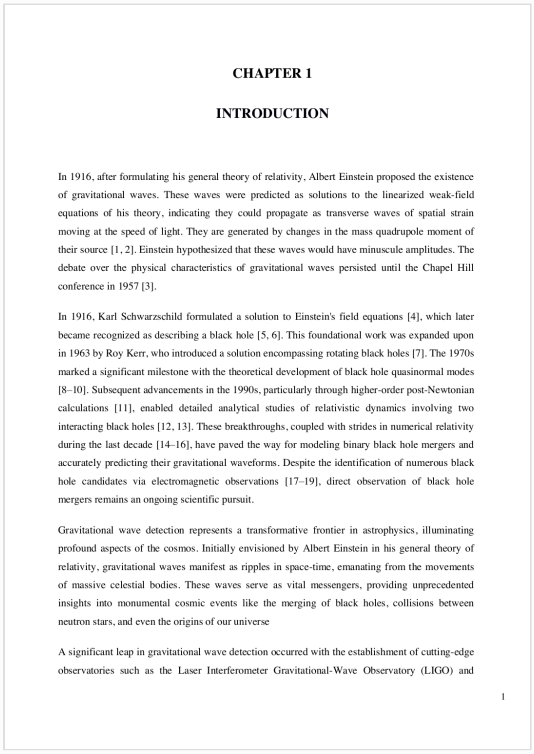

CHAPTER 1

INTRODUCTION

In 1916, after formulating his general theory of relativity, Albert Einstein proposed the existence of gravitational waves. These waves were predicted as solutions to the linearized weak-field equations of his theory, indicating they could propagate as transverse waves of spatial strain moving at the speed of light. They are generated by changes in the mass quadrupole moment of their source [1, 2]. Einstein hypothesized that these waves would have minuscule amplitudes. The debate over the physical characteristics of gravitational waves persisted until the Chapel Hill conference in 1957 [3].

In 1916, Karl Schwarzschild formulated a solution to Einstein's field equations [4], which later became recognized as describing a black hole [5, 6]. This foundational work was expanded upon in 1963 by Roy Kerr, who introduced a solution encompassing rotating black holes [7]. The 1970s marked a significant milestone with the theoretical development of black hole quasinormal modes [8–10]. Subsequent advancements in the 1990s, particularly through higher-order post-Newtonian calculations [11], enabled detailed analytical studies of relativistic dynamics involving two interacting black holes [12, 13]. These breakthroughs, coupled with strides in numerical relativity during the last decade [14–16], have paved the way for modeling binary black hole mergers and accurately predicting their gravitational waveforms. Despite the identification of numerous black hole candidates via electromagnetic observations [17–19], direct observation of black hole mergers remains an ongoing scientific pursuit.

Gravitational wave detection represents a transformative frontier in astrophysics, illuminating profound aspects of the cosmos. Initially envisioned by Albert Einstein in his general theory of relativity, gravitational waves manifest as ripples in space-time, emanating from the movements of massive celestial bodies. These waves serve as vital messengers, providing unprecedented insights into monumental cosmic events like the merging of black holes, collisions between neutron stars, and even the origins of our universe

A significant leap in gravitational wave detection occurred with the establishment of cutting-edge observatories such as the Laser Interferometer Gravitational-Wave Observatory (LIGO) and

1

QCNN

ORIGINALITY REPORT

20%	15%	13%	7%
SIMILARITY INDEX	INTERNET SOURCES	PUBLICATIONS	STUDENT PAPERS

PRIMARY SOURCES

1	123dok.org Internet Source	3%
2	fastercapital.com Internet Source	1%
3	Hilal Ahmad Bhat, Farooq Ahmad Khanday, Brajesh Kumar Kaushik, Faisal Bashir, Khurshed Ahmad Shah. "Quantum Computing: Fundamentals, Implementations and Applications", IEEE Open Journal of Nanotechnology, 2022 Publication	1%
4	www.pure.ed.ac.uk Internet Source	1%
5	arxiv.org Internet Source	1%
6	www.science.gov Internet Source	1%
7	GERALDINE NEWTON-CROSS. "Modelling the distribution of badgers Meles meles: comparing predictions from field-based and	<1%

ACKNOWLEDGEMENT

The satisfaction and joy that accompany the successful completion of any task would be incomplete without the mention of those who made it possible. I would like to thank the supportand guidance that came from various quarters during the course of my project work.

With the showers of blessing of God, I kept fit enough throughout the project for its successful completion. I submit my success and my project work and myself to the Almighty.

First of all, I thank to **Dr. N S Sreekanth,** Head of the Department of IT, for his valuable suggestion and guidance and for providing the necessary facilities.

I would like to express my thanks to **Dr. R K Sunil Kumar** (Assistant Professor, Kannur University, Mangattuparamba Campus) and **Mr. Ebin Antony** (Faculty of Department IT, Kannur University, Mangattuparamba Campus) for giving me such an opportunity. I would also like to remember their support and guidance during my project period.

I am extremely grateful **Ms.Shylaja P, other faculties** for their inspiring guidance and constant encouragement during the project period that enabled me to complete my work successfully.

My acknowledgement would not be complete without acknowledging my gratitude to my beloved parents who have been the pillars of support and constant encouragement throughout the course of this project.

VYSHNAV K P

ABSTRACT

Gravitational wave detection has significantly advanced our comprehension of the universe, revealing deep insights into some of its most potent and mysterious phenomena. In this study, we propose a novel method employing Quantum Convolutional Neural Networks (QCNNs) to classify gravitational wave signals into binary categories. Our objective is to illustrate the efficacy of QCNN architectures in precisely identifying these cosmic signals. While conventional approaches have predominantly used classical algorithms, our research seeks to evaluate the performance and potential benefits of QCNN architectures in the realm of gravitational wave detection. QCNNs utilize quantum mechanical principles like superposition and entanglement to execute computations beyond the capabilities of classical networks. We introduce thermal noise into the data, assess its effects, and subsequently remove it using Wiener filtering and Bayesian inference techniques. We thoroughly examine these denoising strategies to identify the most effective method for noise elimination. Through comprehensive analysis and meticulous experimentation, we investigate the unexplored potential of QCNNs in signal classification tasks, thereby contributing to the advancement of techniques in gravitational wave detection.

TABLEOFCONTENTS

CHAPTER 1

INTRODUCTION

In 1916, after formulating his general theory of relativity, Albert Einstein proposed the existence of gravitational waves. These waves were predicted as solutions to the linearized weak-field equations of his theory, indicating they could propagate as transverse waves of spatial strain moving at the speed of light. They are generated by changes in the mass quadrupole moment of their source [1, 2]. Einstein hypothesized that these waves would have minuscule amplitudes. The debate over the physical characteristics of gravitational waves persisted until the Chapel Hill conference in 1957 [3].

In 1916, Karl Schwarzschild formulated a solution to Einstein's field equations [4], which later became recognized as describing a black hole [5, 6]. This foundational work was expanded upon in 1963 by Roy Kerr, who introduced a solution encompassing rotating black holes [7]. The 1970s marked a significant milestone with the theoretical development of black hole quasinormal modes [8–10]. Subsequent advancements in the 1990s, particularly through higher-order post-Newtonian calculations [11], enabled detailed analytical studies of relativistic dynamics involving two interacting black holes [12, 13]. These breakthroughs, coupled with strides in numerical relativity during the last decade [14–16], have paved the way for modeling binary black hole mergers and accurately predicting their gravitational waveforms. Despite the identification of numerous black hole candidates via electromagnetic observations [17–19], direct observation of black hole mergers remains an ongoing scientific pursuit.

Gravitational wave detection represents a transformative frontier in astrophysics, illuminating profound aspects of the cosmos. Initially envisioned by Albert Einstein in his general theory of relativity, gravitational waves manifest as ripples in space-time, emanating from the movements of massive celestial bodies. These waves serve as vital messengers, providing unprecedented insights into monumental cosmic events like the merging of black holes, collisions between neutron stars, and even the origins of our universe

A significant leap in gravitational wave detection occurred with the establishment of cutting-edge observatories such as the Laser Interferometer Gravitational-Wave Observatory (LIGO) and

Virgo. These advanced facilities employ intricate interferometers spanning kilometers, enabling the direct detection of subtle distortions in space-time induced by passing gravitational waves. Since their landmark detection in 2015, gravitational waves have unveiled a plethora of cosmic phenomena, confirming enduring theoretical hypotheses and forging new avenues in astronomical inquiry.

Gravitational wave astronomy has evolved into a cornerstone of modern astrophysics, offering pivotal insights into the celestial events responsible for these elusive signals. The precise identification and classification of gravitational wave signatures are paramount for unraveling their astrophysical origins. While classical algorithms have historically served this purpose well, they are constrained by inherent limitations. With advancements in gravitational wave detector sensitivity and the exponential growth of observational data, there is an escalating demand for computational methods that are not only more efficient but also robust enough to handle the intricate, high-dimensional data characteristic of gravitational wave signals.

Machine learning algorithms, particularly Convolutional Neural Networks (CNNs), have demonstrated exceptional capabilities in tasks such as image recognition and natural language processing by effectively leveraging data correlations. However, CNNs face challenges in efficiently learning from data or models with excessively large dimensions, limiting their performance in these scenarios.

Traditional methods for detecting gravitational waves have relied on classical algorithms and conventional signal processing techniques. While these methods have been effective, there is increasing interest in advanced computational approaches to enhance detection accuracy and efficiency. Quantum machine learning (QML) integrates quantum computing principles with traditional machine learning techniques, leveraging the computational power of quantum systems for data-driven tasks. In QML, quantum algorithms process information, and among these cutting-edge techniques is the Quantum Convolutional Neural Network (QCNN). QCNNs use quantum counterparts of classical neural network components, significantly improving the ability to handle and classify data with greater efficiency and effectiveness in gravitational wave detection.

QCNNs are inspired by classical convolutional neural networks (CNNs), which are extensively used in tasks like image and signal processing. However, QCNNs leverage the unique advantages of quantum computing to process and analyze data in fundamentally different ways. They hold promise for improving the performance of machine learning models, especially in scenarios

involving high-dimensional and complex datasets. Our research explores the application of QCNNs to the binary classification of gravitational wave signals. We aim to evaluate whether QCNN architectures can effectively identify these cosmic signals and compare their performance against traditional classical algorithms. This investigation seeks to reveal the potential benefits of quantum-inspired computational techniques in enhancing the accuracy and efficiency of gravitational wave detection.

The detection process is often complicated by the presence of thermal noise, which can obscure gravitational wave signals. To address this, we incorporate thermal noise into our dataset and apply advanced denoising techniques, specifically Wiener filtering and Bayesian inference methods. By rigorously analysing these techniques, our goal is to identify the most effective method for mitigating noise and enhancing signal clarity.

We will evaluate the performance of QCNNs based on accuracy, computational efficiency, and scalability. Additionally, we aim to uncover any potential benefits or limitations of quantum-inspired techniques in this domain. To train and validate our models, we will utilize the G2Net dataset, a publicly available repository of simulated gravitational wave signals. The Tensor Flow Quantum (TFQ) platform will serve as our computational framework, offering a seamless interface for developing and deploying quantum-inspired machine learning models. This research also aims to verify whether the QCNN model is capable of more efficient learning compared to CNNs. By leveraging the G2Net dataset on the Tensor Flow Quantum platform, we will rigorously assess and compare the learning capabilities and overall performance of QCNNs and CNNs in the context of gravitational wave signal detection.

CHAPTER 2

LITERATURE REVIEW

In their seminal work titled "Machine Learning for Gravitational-Wave Detection Surrogate: Wiener Filtering for the Prediction and Optimized Cancellation of Newtonian Noise at Virgo" [20], F. Badaracco et al. (2020) introduce a pioneering use of machine learning to improve gravitational-wave detection. Their method focuses on optimizing seismometer array configurations to effectively reduce Newtonian noise, a major challenge in gravitational-wave detectors. By training a surrogate model of a Wiener filter, their approach identifies optimal sensor setups, enhancing noise cancellation particularly in seismic environments with sparse sensor coverage.

This research represents a significant contribution to the intersection of machine learning and astrophysics, where advanced computational techniques are increasingly employed to enhance the precision and sensitivity of gravitational-wave detectors. Recent advancements have witnessed a surge in the application of machine learning techniques across various facets of gravitational-wave detection, including signal processing, noise reduction, event classification, and parameter estimation. By harnessing artificial intelligence, researchers aim to elevate the sensitivity and accuracy of gravitational-wave detectors, thereby expanding our comprehension of cosmic phenomena and pushing the boundaries of astrophysical exploration.

In their study titled "Detection and Parameter Estimation of Gravitational Waves from Binary Neutron-Star Mergers in Real LIGO Data Using Deep Learning" [21], Plamen G. Krastev et al. (2021) employ deep neural networks to detect and analyze gravitational wave signals originating from binary neutron-star mergers within actual LIGO data. By training these networks on a combination of simulated and real observational data, the research demonstrates the efficacy of artificial neural networks in swiftly identifying specific signals amidst noise and accurately estimating their parameters. This approach marks a significant advancement in leveraging deep learning for gravitational-wave astronomy, promising improved sensitivity and precision in detecting cosmic events.

Krastev's study represents a significant leap forward in gravitational wave astronomy, showcasing how deep learning techniques can revolutionize the detection and characterization of gravitational

wave signals from binary neutron-star mergers. Leveraging artificial neural networks enables researchers to gain unprecedented insights into the universe's most energetic events, thereby pushing the boundaries of our understanding of cosmic phenomena.

In his **2021** study titled "Detecting Gravitational Waves by Combining the Constant-Q Transform with Convolutional Neural Networks (CNNs)" [22], **Dingyun Zhang** proposed an innovative approach using deep learning. The constant-Q transform, renowned for its high frequency-resolution properties, preprocesses gravitational wave signals to prepare them for analysis using Convolutional Neural Networks (CNNs). Zhang's method integrates these two techniques to address significant challenges in gravitational wave detection.

Gravitational waves are exceedingly faint signals often obscured by noise, traditionally detected through template matching where observed signals are compared to precomputed templates of expected waveforms. However, this approach can be computationally intensive and less effective for signals that deviate from the templates. Leveraging CNNs' robust pattern recognition capabilities, Zhang's approach achieved notable success, demonstrating a high Area Under the Curve (AUC) score and achieving top-tier rankings on the Kaggle leader board. This study underscores the effectiveness of combining advanced signal processing techniques with deep learning methodologies to enhance sensitivity and accuracy in detecting gravitational wave signals.

In his ground-breaking study titled "Translating Neutron Star Observations to Nuclear Symmetry Energy via Deep Neural Networks" [23], **Plamen G. Krastev (2022)** explores the application of deep neural networks to interpret neutron star observables in the context of nuclear symmetry energy. Neutron stars, renowned for their extreme densities and gravitational fields, provide unique insights into the properties of dense nuclear matter. However, extracting crucial nuclear characteristics from observational data presents challenges that necessitate advanced analytical techniques and theoretical frameworks.

Krastev and his team employ deep learning to directly deduce the equation of state and other pertinent nuclear matter properties from neutron star observations. By training deep neural networks on observational data gathered from missions like NICER (Neutron Star Interior Composition Explorer) and gravitational wave detectors such as LIGO/VIRGO/KAGRA, their study demonstrates the capability to accurately correlate neutron star observables—such as masses, radii, and tidal deformabilities—with the nuclear symmetry energy with unprecedented

precision. This novel approach signifies a significant leap forward in comprehending neutron star physics and nuclear astrophysics through the integration of machine learning methodologies.

In their study titled "Optimized Detection of Continuous Gravitational-Wave Signals using Convolutional Neural Networks" [24], **Premkumar Duraisamy et al. (2023)** expanded the application of convolutional neural networks (CNNs) to time-series data for more effective gravitational wave detection. Their methodology involved utilizing Fourier transformation to convert time-domain signals into the frequency domain, enabling the extraction of subtle signal features. By integrating CNNs with frequency-domain representations, the study achieved enhanced accuracy in identifying gravitational wave signals.

The frequency-domain graphs were particularly adept at capturing the unique characteristics inherent in these signals. This research underscores the significance of employing appropriate signal transformation techniques to bolster detection performance. Moreover, it underscores the adaptability of CNNs in handling intricate datasets and highlights their potential to propel advancements in gravitational wave detection through innovative computational approaches.

In his 2023 study, titled "A Deep Learning Approach to Extracting Nuclear Matter Properties from Neutron Star Observations" [25], **Plamen G. Krastev** explores a novel method to derive nuclear matter properties directly from observational data obtained from neutron stars, which are remnants of supernova explosions characterized by extreme density. Traditionally, analysing neutron star observations has relied on complex theoretical models and assumptions, introducing uncertainties in determining fundamental nuclear properties.

Krastev's study addresses these challenges by leveraging deep learning techniques trained on a combination of observational data and simulated scenarios. This approach successfully demonstrates the ability to accurately extract properties such as the slope, curvature, and skewness of nuclear symmetry energy at saturation density. This advancement not only deepens our understanding of dense neutron-rich matter but also underscores the robustness and efficiency of deep learning as a tool for extracting crucial information in the dynamic field of multi-messenger astrophysics.

Judith Herrmann (2024) addressed the challenge of detecting continuous gravitational waves (CGWs) using a machine learning approach that relied on synthetic training data [26]. Given the difficulty posed by the faintness of gravitational wave signals and pervasive noise, Herrmann employed synthetic training data to enhance their model's accuracy. By integrating machine

learning techniques with high-quality synthetic data, the study achieved high levels of accuracy during training and demonstrated compatibility with advanced image classifiers. This research marks a significant advancement in distinguishing weak gravitational wave signals from background noise, underscoring the effectiveness of data-driven methods in tackling complex problems in astrophysics.

Improving gravitational-wave detection using machine learning involves key areas for enhancing accuracy, efficiency, and applicability. Firstly, robustness against noise and uncertainties in observational data is critical, requiring algorithms that differentiate genuine signals from noise sources like instrument artifacts and environmental disturbances. Secondly, optimizing computational efficiency is essential as datasets grow, enabling faster data processing and real-time analysis for timely event detection. Additionally, integrating advanced quantum computing techniques such as QCNNs offers potential for quantum advantage in precise parameter estimation and deeper astrophysical insights. Collaborative efforts across astrophysics, machine learning, and quantum computing will drive these advancements, paving the way for transformative discoveries in gravitational-wave astronomy.

CHAPTER 3

QUANTUM COMPUTING

Quantum Computing stands at the forefront of technological innovation, poised to overcome the constraints of traditional CMOS technology, particularly in high-density and high-performance applications. This transformative potential has captured the interest of researchers worldwide, although the quantum properties it harnesses present a steep learning curve for newcomers. Unlike conventional processors that encode information into binary bits (0s and 1s) and process data sequentially using logic gates built from switching transistors, quantum computing operates on fundamentally different principles.

Current computing systems rely on classical physics, leveraging semiconductor transistors until they approach atomic dimensions. In 1975, Gordon Moore forecasted that the number of transistors on integrated circuits would double every eighteen months. Projections suggest that in the coming decade, the clock frequency of current computer processors could potentially reach up to 40 GHz. However, as technology advances and these scales are approached, classical physics may no longer suffice. This prompts exploration into new models based on quantum mechanics, such as quantum computing, which is gaining increasing attention for its potential to overcome these limitations.

Quantum computing has garnered substantial interest from major players in the industrial sector, including tech giants like Microsoft and Google. Additionally, companies traditionally focused on nanoelectronics and nanotechnology, such as IBM and Intel, are also heavily invested in advancing quantum computing technologies.

Quantum computers leverage qubits, which unlike classical bits, can exist in multiple states simultaneously through superposition. These qubits are realized at the atomic level using atoms, photons, ions, or electrons, integrated with control devices to serve as processors and memory units. Researchers have explored various implementations, including solid-state qubits like Josephson junctions in superconductors and spin qubits in silicon, which are scalable and compatible with existing CMOS technology.

The ability of qubits to process and store vast amounts of data simultaneously grants quantum computers immense computational power, potentially surpassing today’s top supercomputers by millions of times. Moreover, quantum computers offer advantages such as ultra-secure data

transmission, exceptionally high processing speeds, and the capacity to store significantly larger volumes of information compared to classical computers. These capabilities make quantum computing a promising frontier for solving complex problems in science, engineering, and cryptography.

3.1 Quantum Computing Systems

Quantum computation and quantum information are focused on harnessing quantum mechanical systems for information processing tasks, constituting a branch of quantum information science. At the heart of computing lies the manipulation and storage of information. While traditional computers manipulate individual bits, quantum computers exploit quantum phenomena like superposition and entanglement to encode data as quantum bits (qubits). Unlike classical bits, qubits can exist in a simultaneous state of 0 and 1 due to superposition.

This unique capability enables a set of qubits to represent exponentially more information than an equivalent set of classical bits, making quantum computing a highly promising platform. It has the potential to solve complex computational problems that are currently beyond the capabilities of even the most advanced classical supercomputers. Quantum computing holds the key to unlocking new frontiers in cryptography, materials science, drug discovery, and optimization, offering unprecedented computational power and efficiency.

3.2 Qubits Vs Bits

In quantum computing, the basic unit of information is the qubit, which is fundamentally different from the classical bit. While a classical bit can only be in one of two states—either 0 or 1—a qubit can exist in a superposition of both states simultaneously. Mathematically, a qubit is represented as:

$$\Psi = \alpha\,|0\rangle + \beta\,|1\rangle$$

Equation-1

Here, α and β are probability amplitudes that can, in general, be complex numbers. The condition that ensures the qubit is in a valid quantum state is:

$$\alpha^2 + \beta^2 = 1 \text{ (Equation -2)}$$

In a two-dimensional complex vector space, the state of a qubit can be generalized as a vector. The special states |0⟩ and |1⟩, known as computational basis states, form an orthonormal basis for this vector space. These basis states are represented as follows:

$$|0\rangle = (0, 1) \text{ and } |1\rangle = (1, 0)$$

In this representation, |0⟩ and |1⟩ are orthogonal to each other, meaning their inner product is zero, and they are normalized, meaning each has a magnitude of one. This orthonormality is crucial for defining qubit states and performing quantum computations.

One useful way to visualize the evolution of a qubit state is through a geometric representation of the pure state space of a two-level quantum mechanical system. This representation, known as the Bloch sphere, is named after the physicist Felix Bloch. The Bloch sphere provides an intuitive way to understand the state of a qubit and its transformations. In this model, any pure qubit state can be represented as a point on the surface of a sphere, as illustrated in Figure 3.2.1

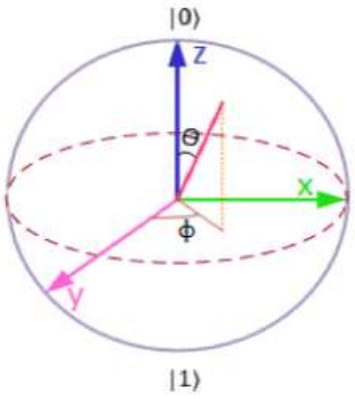

Figure 3.2.1 Qubit Vs Bits

The north pole of the sphere represents the state |0⟩.

The south pole represents the state |1⟩.

Any other point on the surface of the sphere corresponds to a superposition of |0⟩ and |1⟩.

The Bloch sphere helps in visualizing the qubits behaviour under various quantum operations and transformations, making it a powerful tool for understanding quantum mechanics.

3.3 Representation of Qubits

In quantum mechanics, and similarly in quantum computing, states are often described using Dirac notation [44] because it provides a much more concise representation compared to matrices. In Dirac notation, vectors are represented as "kets." For instance, a vector "a" would be denoted as $|a\rangle$. Conversely, dual vectors are expressed using "bras," so the dual vector "b" would be $\langle b|$.

Alternatively, matrix representation, as indicated in (3), signifies the probabilities associated with a qubit being in specific states. In this matrix:

the top entry corresponds to the probability amplitude of the qubit collapsing to state 0, while the bottom entry represents the probability amplitude of collapsing to state 1. This matrix form is essential for computational operations in quantum mechanics and quantum computing, providing insights into the probabilities and behaviors of quantum states.

$$0 = \begin{bmatrix} 1 \\ 0 \end{bmatrix}; 1 = \begin{bmatrix} 0 \\ 1 \end{bmatrix}$$

Equation (3)

Matrix representations for 0 and 1. Equation (4) illustrates how a single qubit's overall state is shown in both matrix form and Dirac notation.

$$|\Psi\rangle = \alpha_0 |0\rangle + \alpha_1 |1\rangle = \begin{bmatrix} \alpha_0 \\ \alpha_1 \end{bmatrix}$$
$$|\alpha_0|^2 + |\alpha_1|^2 = 1$$

Equation (4)

Where α_0 and α_1 are complex numbers representing the probability amplitudes of state vectors, ensuring their squared absolute values sum up to one. This principle extends to systems with multiple qubits, where each qubit contributes a complex entry, subject to the same normalization condition across all possible states. Importantly, these interconnected probability amplitudes reflect the inherent uncertainty of quantum states, where a qubits final state "collapses" to one of the possible outcomes upon measurement. For further detailed explanations on qubit processing, refer to [45].

3.4 Superposition and Entanglement

Superposition and entanglement are fundamental concepts in quantum mechanics, particularly when examining microscopic particles like photons, atoms, and electrons. Superposition refers to the ability of a quantum system to occupy multiple states simultaneously. This means that an object can exist in multiple states, such as being "here" and "there," or simultaneously "up" and "down." In quantum computing, this property allows qubits to represent both 0 and 1 at the same time. With n qubits, a quantum computer can process 2^n states in parallel, a capability far beyond the reach of classical computers.

Entanglement, on the other hand, describes a unique correlation between quantum particles. When particles become entangled, their states become interconnected regardless of the distance between them. This phenomenon, famously debated by Albert Einstein in 1935, implies that changes to one entangled particle instantaneously affect its partner, even if they are separated by vast distances. Einstein referred to this as "spooky action at a distance," highlighting its mysterious and non-intuitive nature.

Experimental demonstrations have effectively showcased the creation of superposition and entanglement in photonic quantum states, providing tangible evidence of these foundational principles of quantum mechanics.

3.5 Quantum Reversibility and Quantum Gates

Quantum computing relies on the foundational principle of reversible computation, which ensures that the input state can be perfectly reconstructed from the output state without any irreversible loss of information. This concept encompasses both physical reversibility, where no information is lost irreversibly, and logical reversibility, which allows for the exact reconstruction of input from output.

In classical computing, certain logic gates like NAND are inherently irreversible because they map multiple inputs to a single output, making it impossible to uniquely determine the inputs from the outputs. Conversely, gates like NOT are reversible because each input state corresponds to a unique output state, and vice versa.

Quantum gates form the basic building blocks of quantum circuits, manipulating qubits to perform quantum computations. These gates include single-qubit operations such as H (Hadamard), X (Pauli-X), Y (Pauli-Y), Z (Pauli-Z), T, I (identity), and Phase gate. Crucially, two-qubit gates like CNOT (controlled-NOT), CZ (controlled-Z), and Swap gate play essential roles. For operations involving three qubits, gates like Toffoli and Fredkin are utilized.

Furthermore, quantum circuits have the capability to simulate classical logic gates such as NAND, NOR, OR, AND, and XOR using combinations of single-qubit and two-qubit quantum gates. These quantum logic gates are mathematically described by unitary matrices, where a gate operating on n qubits corresponds to a $2^n \times 2^n$ unitary matrix. This matrix ensures that the quantum operation maintains the superposition and entanglement states of the qubits, enabling sophisticated computations within quantum computing architectures.

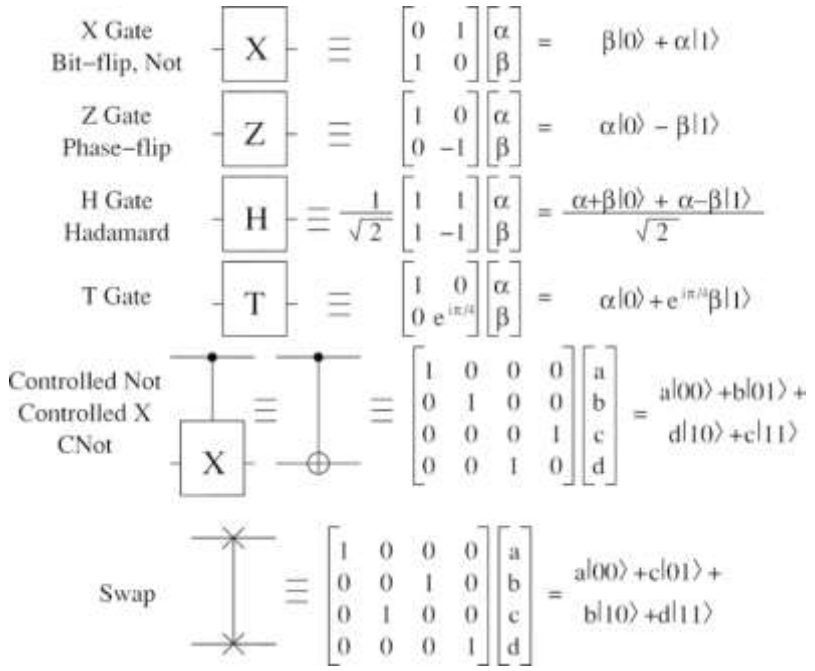

Figure 3.5.1 Quantum gates

3.6 Quantum Machine Learning

Quantum Machine Learning (QML) is an emerging interdisciplinary field that integrates principles from quantum computing and machine learning to create algorithms capable of

processing and analyzing data using quantum mechanics. Unlike classical machine learning algorithms that rely on bits (which are binary, either 0 or 1), QML algorithms utilize quantum bits or qubits. Qubits can exist in superposition states, allowing them to represent both 0 and 1 simultaneously, and they can be entangled with each other, enabling parallel computations and potentially exponential speedups in certain tasks. QML harnesses key quantum principles like superposition and entanglement to perform computations. Superposition enables qubits to hold multiple states at once, while entanglement establishes correlations between qubits that can enhance computational efficiency. The goal of QML is to develop quantum algorithms that surpass classical methods in tasks such as optimization, pattern recognition, and data analysis. Examples include quantum adaptations of support vector machines, clustering algorithms, and neural networks tailored for quantum environments.

As quantum computing technologies have advanced, researchers have increasingly focused on crafting quantum algorithms specifically designed for machine learning tasks. Early algorithms such as Grover's algorithm for database search and quantum support vector machines (QSVMs) for classification have demonstrated quantum computing's potential advantages in tasks like pattern recognition, optimization, and data analysis. These advancements underscore quantum computing's capability to outperform classical approaches in specific computational tasks critical to the field of machine learning.

The journey of integrating quantum computing with machine learning is driven by the quest for faster computations, enhanced data processing capabilities, and breakthroughs in complex problem-solving. From theoretical foundations and algorithmic developments to interdisciplinary collaborations and overcoming hardware challenges, each step advances our understanding and application of quantum-enhanced machine learning. As quantum technologies continue to evolve, they promise to unlock new possibilities and transform industries through innovative quantum computing applications in machine learning.

Quantum Convolutional Neural Networks (QCNNs) represent a cutting-edge advancement at the intersection of quantum computing and deep learning, pushing the boundaries of computational intelligence. Combining principles from quantum mechanics with the architecture of traditional convolutional neural networks (CNNs), QCNNs aim to harness quantum phenomena like superposition and entanglement to revolutionize machine learning tasks.

The journey of QCNNs begins with the foundational developments in both quantum computing and neural networks. Quantum computing emerged in the 1980s, pioneered by physicists like

Richard Feynman and David Deutsch, who theorized about quantum algorithms and the potential of quantum information theory to surpass classical computing limits. This era laid the groundwork for exploring quantum states where bits could exist simultaneously in multiple states (superposition) and become intricately correlated (entangled), fundamentally altering how computations could be performed.

Simultaneously, the evolution of neural networks from their inception in the 1940s to the development of CNNs in the 1980s and 1990s by pioneers such as “Yann LeCun” marked a significant milestone in machine learning. CNNs revolutionized tasks like image recognition by leveraging hierarchical feature extraction through convolutional layers, drastically improving accuracy and efficiency in processing visual data.

The convergence of quantum computing and neural networks to form QCNNs emerged in the 21st century as researchers sought ways to exploit quantum advantages in machine learning tasks. QCNNs are designed to extend the capabilities of classical CNNs by processing data using quantum states of qubits. In a QCNN, quantum convolutional layers operate similarly to their classical counterparts, applying filters to input data to extract features. However, instead of classical bits, QCNNs use qubits that can simultaneously represent all possible states due to superposition, exponentially increasing the computational power and efficiency for tasks such as pattern recognition and data classification.

The working principles of QCNNs hinge on quantum gates, analogous to classical neural network operations but executed on quantum states. Quantum gates manipulate qubits based on unitary matrices, performing operations such as quantum convolutions, pooling, and activation functions. These gates exploit quantum coherence and entanglement to process information in parallel across vast numbers of potential states, offering a potential quantum advantage in complex computational tasks.

Training QCNNs involves adapting quantum circuits to learn from data, a process known as quantum circuit learning. This approach combines classical optimization techniques with quantum algorithms to adjust the parameters within quantum circuits, optimizing the network's performance based on specific learning objectives. Hybrid quantum-classical algorithms are often employed to mitigate quantum errors and enhance the stability of computations, ensuring reliable and accurate outcomes.

Applications of QCNNs span diverse fields where quantum-enhanced machine learning can offer transformative capabilities. In fields like quantum chemistry, QCNNs promise to accelerate simulations of molecular interactions and drug discovery processes by efficiently processing large datasets and identifying complex patterns in molecular structures. Similarly, in finance, QCNNs can enhance predictive modeling and risk assessment by leveraging quantum parallelism to analyze vast amounts of financial data and detect subtle market trends or anomalies.

the development of QCNNs faces challenges such as qubit coherence times, gate fidelity, and scalability limitations in current quantum hardware. Researchers are actively addressing these challenges through advancements in quantum error correction, noise reduction techniques, and the development of more robust quantum algorithms tailored for specific applications. As quantum computing technologies continue to mature, QCNNs hold the promise of revolutionizing artificial intelligence and computational science by unlocking new realms of quantum-enhanced machine learning capabilities.

Quantum Convolutional Neural Networks represent a pivotal advancement in the synergy between quantum computing and deep learning, offering unprecedented potential to solve complex computational problems that classical computers struggle to handle efficiently. The ongoing research and development in QCNNs underscore their role in shaping the future of quantum-enhanced machine learning, marking a significant milestone in the evolution of computational intelligence and artificial intelligence technologies.

CHAPTER 4

GRAVITATIONAL WAVE

In the early 2000s, our understanding of the universe took significant strides forward with pivotal discoveries. Among these, the detection of the double pulsar PSR J0737-3039 in 2003 [27–28] marked a breakthrough in astrophysics, offering unprecedented insights into the dynamics of compact binary systems. This system not only provided a unique laboratory for testing theories of gravity but also confirmed predictions of General Relativity in the strong-field regime. Another notable achievement came in 2013 with the observation of PSR J0348+0432, a binary system featuring a closely-orbiting pair consisting of a newly discovered pulsar and a white dwarf companion. The extreme conditions within this system rigorously tested Einstein's equations, particularly in relation to the emission of gravitational radiation, thereby reaffirming the extraordinary precision of General Relativity [29].

A thorough examination of General Relativity necessitates delving into the realm of strong-field gravitational physics. In this regime, mass movements approach the speed of light c,, and gravitational potentials approach c2. In the vicinity of a black hole, characterized by a central singularity surrounded by an event horizon, relativistic gravity exhibits profound effects. Studying phenomena such as the inspiral of a compact object near a black hole's event horizon or the merger of two black holes yields crucial insights into gravity under the extreme conditions of the relativistic strong-field limit.

In 2013, the European Space Agency's Planck mission achieved a significant milestone by confirming the Lambda Cold Dark Matter (ΛCDM) paradigm in cosmology with unprecedented precision [30]. The mission produced an intricate all-sky map that vividly depicted the distribution of dark matter across cosmic evolution. These observations bolstered the understanding that quantum fluctuations, emerging during the inflationary epoch, underwent progressive amplification due to gravitational interactions with dark matter. Over eons, these fluctuations evolved into the colossal cosmic structures seen today, including galaxies harboring billions of stars and central black holes [31].

According to the ΛCDM (Lambda Cold Dark Matter) model, the formation of black holes originated from the initial seeds within dark matter halos through the dissipative collapse of

baryons [32–33]. As these halos aggregated and merged throughout cosmic epochs, their resident black holes also underwent mergers [34–35]. Consequently, binary black holes naturally form as galaxies collide and merge, providing insights into the evolution of cosmic structures. Galaxy mergers were more frequent in the early universe. The subsequent mergers of massive black holes not only serve as a test-bed for theories of gravity and black hole formation but also offer a unique opportunity to study the universe's evolution from its early stages to the present day.

In the year 2000, the discovery of dormant black holes in nearby galaxies, coupled with evidence linking the mass of black holes to the stellar mass of their host galaxies [36–37], introduced the concept of co-evolution between black holes and galaxies. This mutual interaction is reciprocal: black holes influence the evolution of galaxies, while galaxies, in turn, regulate the growth and development of black holes. The merger of binary black holes serves as a precise indicator of galaxy mergers, providing deep insights into the underlying physical mechanisms driving these cosmic processes.

During the early 2000s, numerous ultra-compact binary systems containing white dwarfs and/or neutron stars were identified within our own Milky Way galaxy [38]. These systems offer invaluable opportunities to study the extremes of stellar evolution within binary configurations. Scientists anticipate that some of these systems will undergo transitions leading to Type Ia supernovae or merging binaries-events that ground-based gravitational wave detectors like LIGO and VIRGO are poised to detect in the coming years. However, binary systems consisting of a stellar-mass black hole paired with a pulsar companion remain rare and difficult to detect.

Tracking the nearly invisible ultra-compact binaries of various types across the Milky Way using gravitational waves presents a distinctive opportunity to unravel the formation and evolution of binary stars within both the galaxy's disk and halo. Many of these systems have already been detected through electromagnetic observations, establishing confirmed sources that can be further studied using gravitational wave data. This dual approach not only deepens our comprehension of stellar evolution but also sheds light on the intricate dynamics governing binary star systems throughout the Milky Way.

Using electromagnetic radiation as our primary tool for observation has indeed led to significant advancements in our understanding of the universe, particularly in studying the interactions of baryonic matter. However, a substantial part of the cosmos remains elusive to electromagnetic

detection. On cosmic scales, gravity emerges as the principal force governing the evolution of the universe. Gravitational wave detection offers a transformative extension of our observational capabilities beyond the limits of electromagnetic radiation alone. By detecting gravitational waves, we can explore phenomena and celestial objects that are invisible to traditional telescopes, thereby unlocking new insights into the dynamics and evolution of the universe. This approach promises to broaden our understanding of cosmic processes and unveil previously inaccessible aspects of the cosmos.

Gravitational waves serve as a direct means to observe the universe, manifesting as distortions in the fabric of space-time that propagate at the speed of light and interact weakly with matter, allowing them to traverse immense cosmological distances with minimal attenuation. These waves exhibit a distinctive feature: a fractional stretching and squeezing of space-time perpendicular to their direction of travel, typically characterized by amplitude around 10^-20. Over the past three decades, laser interferometry has emerged as the leading technology for detecting these extremely subtle distortions [39].

Electromagnetic observations of the universe, supported by theoretical models, indicate that the most intriguing portion of the gravitational wave spectrum lies within the frequency range accessible to space interferometers, spanning approximately from 0.1 mHz to 100 mHz. This frequency band presents crucial opportunities to explore the formation of binary star systems within our Milky Way and to investigate cosmic history up to redshifts of around z~20. Such studies enable tests of gravity in the robust strong-field regime and at the TeV energy scale prevalent in the early universe [40].

The eLISA mission represents a ground-breaking endeavour as the first mission designed to survey the entire universe using gravitational waves, under the scientific theme known as "The Gravitational Universe." This ambitious mission concept builds upon the Next Gravitational Observatory (NGO), which ESA studied as a candidate for its L1 mission selection, thereby setting the stage for its further development [39].

4.1 Theory of General Relativity

Einstein's theory of general relativity, first published in 1915, represented a significant extension of his earlier theory of special relativity from 1905, which united space and time into a single framework but did not account for gravity. According to NASA's Glenn Research Center,

gravitational attraction between two objects is determined by both their masses and the distance between them. For example, while the Earth's center pulls objects towards it (keeping them grounded), the objects exert an equal but opposite force on the Earth's center of mass. However, due to their vastly different masses, smaller objects exert negligible gravitational force on the Earth, which keeps them firmly anchored. Newton's laws describe gravity as an inherent force possessed by objects that can influence others over distances.

In contrast, general relativity proposes that massive objects such as planets and stars create a curvature in the fabric of space-time. This curvature affects the paths of objects moving through it, including the trajectory of light. The theory also asserts that gravitational forces are indistinguishable from the effects of acceleration. Put simply, if you were in a sealed environment with no windows and felt a downward force, you would be unable to discern whether it stemmed from gravity or from acceleration through space.

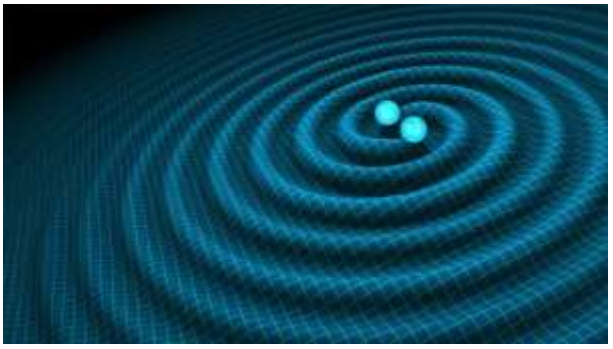

Figure 4.1.1 Colliding black holes

Albert Einstein's theory of special relativity, as articulated by Wired in figure 4.1.1, introduced the principle that the laws of physics are consistent and uniform for all observers in non-accelerating frames of reference. Einstein's groundbreaking work demonstrated that the speed of light remains constant in a vacuum, regardless of the observer's relative motion. This crucial observation prompted him to propose that space and time are interconnected aspects of a unified entity known as space-time. Within the framework of special relativity, events that appear simultaneous to one observer may occur at different times for another observer due to the relativistic effects arising from their relative motion.

In developing his general theory of relativity, Albert Einstein built upon these foundational principles to incorporate the concept of gravity. He postulated that massive objects influence their surroundings by causing a distortion in the fabric of space-time itself. This effect can be likened

to placing a heavy object on a stretched trampoline, which causes a curvature or depression in the fabric. Objects moving near this curved space-time will follow curved paths, analogous to how gravity pulls planets toward stars. Since Einstein's pioneering publications, scientific observations have consistently supported the predictions of relativity. These observations have not only validated but also expanded our understanding of gravity and the intricate nature of space-time over the course of decades.

4.2 What Are Gravitational Waves

Gravitational waves are disturbances in the fabric of space-time, created by some of the universe's most energetic phenomena. Albert Einstein predicted their existence in 1916 as a consequence of his general theory of relativity. These waves emerge when massive objects, such as orbiting neutron stars or black holes, accelerate through space. According to Einstein's equations, this acceleration disrupts space-time, generating ripples that travel outward at the speed of light from their source. These cosmic ripples carry crucial information about their origins, providing insights into the fundamental nature of gravity.

The most powerful gravitational waves stem from cataclysmic events like black hole mergers, the explosive deaths of massive stars called supernovae, and the collisions of neutron stars. Additionally, they can arise from the rotational motion of non-spherical neutron stars and possibly from remnants of gravitational radiation dating back to the universe's early moments during the Big Bang. These waves serve as a ground-breaking tool for observing the cosmos, uncovering hidden aspects of its most violent and profound events.

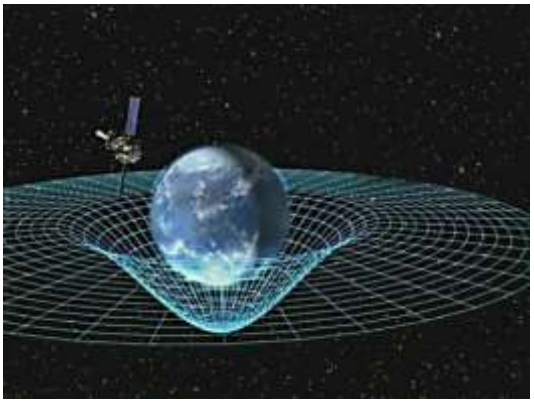

Figure 4.2.1 A two-dimensional depiction of how mass in the Universe bends space-time.

Albert Einstein's prediction of gravitational waves in 1916 received empirical validation in 1974 through a ground-breaking discovery by astronomers Russell Hulse and Joseph Taylor. Using the

Arecibo Radio Observatory in Puerto Rico, they identified a binary pulsar located 21,000 light years from Earth. This pulsar system closely matched the type predicted by Einstein's theory to emit gravitational waves. To test this hypothesis, Taylor, along with colleagues Joel Weisberg and Lee Fowler, meticulously monitored the pulsar's radio emissions over several years to measure changes in its orbital period.

After a thorough four-year observation campaign, they conclusively observed a significant decrease in the orbital period, indicating that the two stars were spiraling closer together at a rate precisely as predicted by general relativity if emitting gravitational waves. The observed rate matched the theoretical prediction with remarkable accuracy, nearly within half a percent. This milestone affirmed a fundamental tenet of Einstein's theory and marked a transformative moment in the field of astrophysics. In recognition of their pioneering work, Hulse and Taylor were jointly awarded the Nobel Prize in Physics in 1993, ushering in a new era for the study of gravity and cosmology.

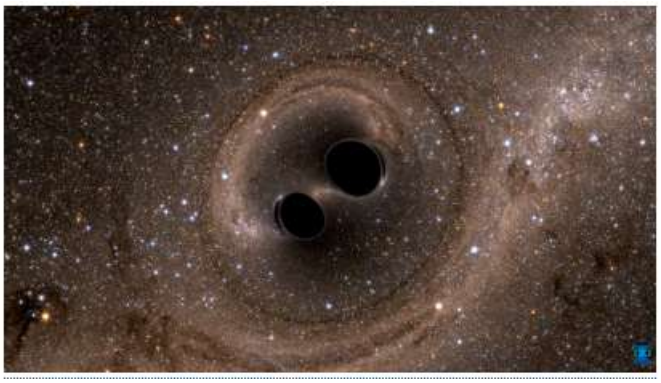

Figure 4.2.2 Merger of binary black holes

Gravitational waves, generated by cataclysmic events such as black hole mergers and neutron star collisions, experience significant attenuation as they travel through the vastness of space. This attenuation occurs because space-time itself resists deformation, causing the waves to diminish exponentially in amplitude over cosmic distances. By the time these waves reach Earth, their effects on space-time are incredibly subtle, approximately 10,000 times smaller than the nucleus of an atom. Detecting such minute distortions poses a major challenge, requiring extraordinarily sensitive instruments like those used by the Laser Interferometer Gravitational-Wave Observatory (LIGO) and Virgo collaborations. These advanced detectors are meticulously crafted to discern the faintest oscillations in space-time caused by passing gravitational waves, enabling scientists to explore cosmic phenomena inaccessible to traditional electromagnetic observatories.

4.3 Massive Binary Black Holes

Exploration of the universe across the electromagnetic spectrum has led to crucial milestones in our comprehension of cosmic history. Observations have unveiled significant events, including the collapse of the most distant star into a stellar-mass black hole, illustrated by the Gamma Ray Burst GRB 090429B at a redshift of approximately z~9.4. This occurrence occurred when the universe was about 520 million years old, affirming that massive stars formed and concluded their lifespans very early in the universe's evolution.

Further remarkable discoveries in cosmology include MACS0647-JD, currently the farthest known galaxy, located at a redshift of approximately z~10.7, when the universe was about 420 million years old. Additionally, ULAS J1120+0641 hosts a supermassive black hole of around 10^9 solar masses, making it the most distant known quasar at a redshift of approximately z~7.08, roughly 770 million years after the Big Bang. These findings underscore the presence of stars, black holes, and galaxies—fundamental constituents of the universe—before the conclusion of the reionization epoch around z~6.

These luminous sources, such as pre-galactic discs, less massive stars, and smaller black holes, represent only a small portion of the diverse cosmic entities whose understanding remains incomplete. Even the brightest quasars diminish in optical visibility due to neutral hydrogen in the intergalactic medium, which causes the Gunn-Peterson trough effect. X-ray searches encounter obstacles such as intrinsic obscuration, crowding, and unresolved background light. The entire range of objects that contributed to the formation of today's larger cosmic structures remains largely unexplored in astronomical research..

During the cosmic dawn, estimated to occur around redshifts z~20–30 in current cosmological models, the universe witnessed the formation of primitive objects. Simulations suggest that these early structures, known as pre-galactic discs, were characterized by their low mass, faint luminosity, and significant deficiency in heavy elements, often described as metal-poor. These discs marked the initial stages of galaxy formation, where gravitational interactions and the collapse of primordial gas clouds set in motion the birth of the first stellar systems. Investigating these early structures is essential for unraveling the origins and evolution of galaxies, as well as understanding the cosmic web that shapes the vast structure of the universe as observed today.

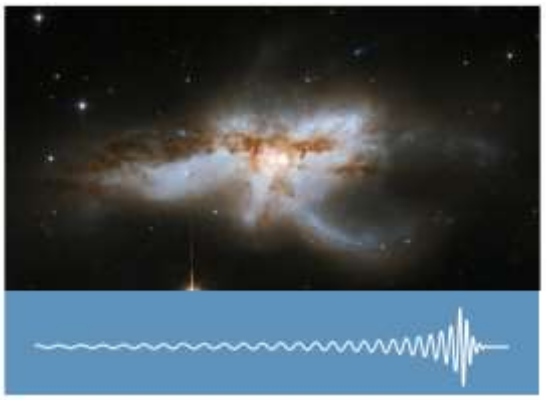

Figure 4.3.1 gravitational waves resulting from the coalescence of two supermassive black holes.

During the period around redshifts z~20 to 30, the earliest stars are believed to have formed with masses exceeding 100 solar masses (M⊙), culminating their lives as stellar-mass black holes. These could have potentially served as the initial seeds for the formation of subsequent supermassive black holes. However, as larger, more massive, and metal-enriched galactic discs emerged over time, alternative pathways for the formation of black hole seeds also became viable. This evolution marked a crucial transition in the cosmic history, influencing the diversity and origins of black holes observed in the universe today.

One pathway involves global gravitational instabilities within gaseous discs, potentially leading to the formation of quasi-stars with masses ranging from 10^3 to 10^4 times that of the Sun (M⊙). These quasi-stars could have collapsed into seed black holes as they evolved. Another scenario includes the collapse of massive stars formed through runaway collisions within young, dense star clusters. Additionally, the collapse of unstable, self-gravitating gas clouds in the cores of gas-rich galaxy mergers during later epochs is considered as another potential pathway for the formation of black hole seeds. These diverse mechanisms illustrate the complex processes that contributed to the formation of black holes across cosmic history.

Therefore, the initial mass of seed black holes stands as a pivotal uncertainty in contemporary theories of black hole formation, owing to the intricate and varied potential formation mechanisms. Moreover, direct detection of individual seed formation events via electromagnetic observations is constrained by current technological limits. Hence, unraveling the origins of these seeds demands a blend of theoretical models, simulations, and forthcoming observational breakthroughs spanning diverse wavelengths in astronomy.

4.4 Ultra-Compact Binaries in the Milky Way

Most stars in the universe reside in binary or multiple star systems, with approximately half of these systems featuring closely orbiting stars that undergo interactions and evolve into compact systems. These compact binaries frequently consist of white dwarfs, neutron stars, or stellar-mass black holes. Notably, ultra-compact binaries with the shortest orbital periods are significant sources of gravitational waves in the millihertz (mHz) frequency range. These gravitational waves offer valuable insights into the dynamics and evolution of these compact stellar systems.

These binary systems typically originate from common-envelope phases, which occur when one star evolves into a giant or supergiant. During this phase, unstable mass transfer leads the stellar core and its companion to spiral closer together, with angular momentum transferred to the giant's extended envelope. Eventually, the envelope is expelled, forming a compact binary system. This process is crucial for the formation of X-ray binaries, binary pulsars, and double white dwarf binaries, which are observed in various states and configurations throughout the Milky Way. Despite their prevalence in our galaxy, only a fraction of these sources are currently comprehensively observed and studied across multiple wavelengths ranging from radio to X-rays.

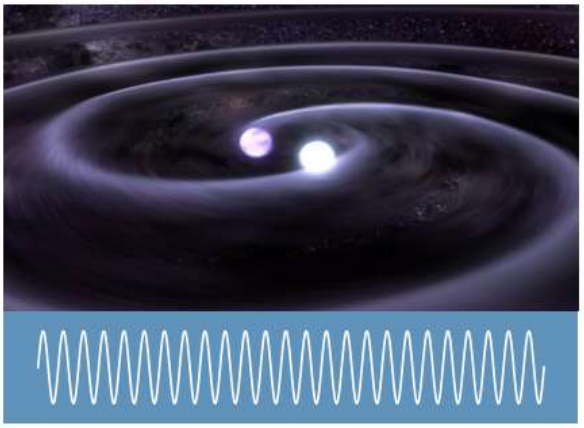

Figure 4.4.1 Illustration depicting a compact binary star system, along with its waveform.

After the common-envelope phase, compact stars within binary systems initially have wider separations but gradually reduce their orbital periods due to the emission of gravitational waves, which causes them to lose angular momentum. As their orbits shrink to durations of minutes or less, depending on the types of compact objects involved, they may undergo additional phases of mass transfer. In the case of binary systems containing two neutron stars, they eventually merge, emitting bursts of high-frequency gravitational waves that could potentially trigger short Gamma-Ray Bursts. Despite theoretical predictions, no binary system involving a neutron star and a

stellar-mass black hole, or two black holes, has been directly observed to date. These elusive events remain highly sought after by gravitational wave observatories, promising to provide crucial insights into the dynamics of extreme astrophysical phenomena.

In binaries containing a white dwarf, the dynamics are governed by a delicate balance between mass loss and angular momentum, often leading to unpredictable outcomes. The dissipation of energy via gravitational waves can drive these systems towards merger, resulting in events such as Type Ia or sub-luminous supernovae, or the formation of rapidly spinning neutron stars resembling millisecond radio pulsars or magnetars.

In a minority of cases, mass transfer can stabilize the binary, leading to the formation of long-lived systems like AM CVn systems (if the companion is a white dwarf) or ultra-compact X-ray binaries (if the companion is a neutron star). This phase of binary evolution involves complex physical processes, including tidal interactions, dynamics of mass transfer, highly super-Eddington accretion, and mechanisms related to mass ejection. These interactions significantly enhance our understanding of stellar evolution and the behavior of compact objects within close binary systems.

4.5 Gravitational Wave Observatories

On September 14, 2015, at 09:50:45 UTC, both detectors of the Laser Interferometer Gravitational-Wave Observatory (LIGO) recorded a transient gravitational-wave signal simultaneously. This signal exhibited a distinctive frequency sweep ranging from 35 to 250 Hz and reached a peak gravitational-wave strain of 1.0 × 10^-21. The observed waveform closely matched the predictions of general relativity for the inspiral, merger, and ring-down phases of a binary black hole system. The detection achieved a matched-filter signal-to-noise ratio (SNR) of 24, indicating high confidence in its authenticity. The event originated from a binary black hole system located at a luminosity distance of 410 +160/-180 mega parsecs (Mpc) from Earth. This distance corresponds to a redshift of z = 0.09 +0.03/-0.04, indicating that the source of the gravitational waves was relatively close in cosmic terms.

The quest to detect gravitational waves began in earnest during the 1960s, sparked by Joseph Weber's pioneering work on resonant mass detectors. Weber's efforts marked the initial steps

toward directly detecting these elusive cosmic ripples, which were originally predicted by Albert Einstein's general theory of relativity in 1916.

A significant breakthrough occurred with the landmark discovery of the binary pulsar system PSR B1913+16 by Russell Hulse and Joseph Taylor in 1974 [40]. Using observations from the Arecibo Radio Observatory, they provided compelling indirect evidence for gravitational waves by confirming that the binary pulsar's orbit was decaying as predicted by general relativity.

Subsequent measurements by Taylor and Weisberg [41] further solidified this evidence, demonstrating the gradual orbital decay of PSR B1913+16 due to energy loss from gravitational wave emission. These findings not only validated Einstein's theory in the weak-field regime but also laid the groundwork for the eventual direct detection of gravitational waves.

Advancements in both astrophysical understanding [42] and technological innovations over subsequent decades culminated in the historic detection of gravitational waves by the Laser Interferometer Gravitational-Wave Observatory (LIGO) in 2015. This landmark discovery marked a transformative moment in astrophysics, ushering in a new era for observing and studying the universe through gravitational waves. It provided unprecedented opportunities to test general relativity in the strong-field regime, particularly in scenarios such as black hole and neutron star mergers.

Building upon Joseph Weber's pioneering work, the field of gravitational wave detection saw significant progress through the development of cryogenic resonant detectors and interferometric detectors. Cryogenic resonant detectors, inspired by Weber's experiments, sought to detect gravitational waves by observing their resonant effects on massive detectors held at extremely low temperatures [43]

4.5.1 Observations

GW150914 signifies the inaugural direct detection of gravitational waves by the Laser Interferometer Gravitational-Wave Observatory (LIGO) on September 14, 2015. This historic event was simultaneously recorded by LIGO's observatories in Hanford, WA, and Livingston, LA. The detected gravitational waves originated from the merger of two black holes located approximately 1.3 billion light-years away from Earth.

The detection of GW150914 was achieved through rapid searches designed to identify transient gravitational-wave events. Within minutes of detection, detailed analysis employing matched-filter techniques confirmed that the observed signal closely matched the theoretical predictions of gravitational waves generated by the inspiral, merger, and ring-down phases of a binary black hole system.

This confirmation was based on comparing the observed signal with relativistic models of compact binary coalescence waveforms. GW150914's detection marked a pivotal moment in astrophysics and gravitational-wave astronomy, providing the first direct evidence of gravitational waves—vibrations in the fabric of space-time as predicted by Albert Einstein's general theory of relativity. This groundbreaking discovery opened up a revolutionary new observational tool to study the universe, offering unprecedented insights into the dynamics of violent and energetic cosmic phenomena that are inaccessible to traditional electromagnetic astronomy methods.

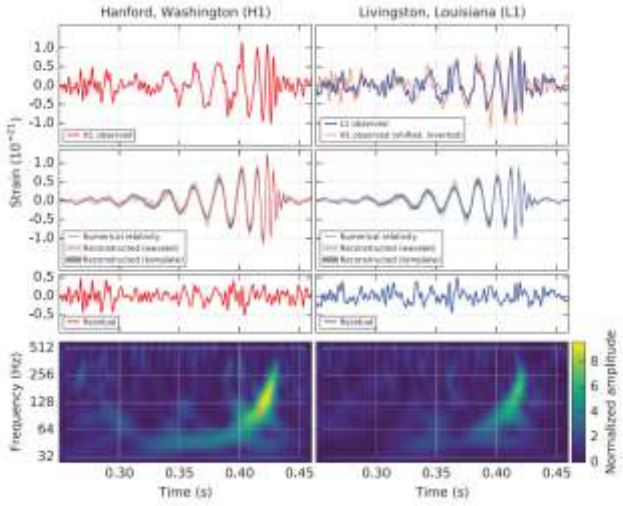

Figure 4.5.1.1 The LIGO Hanford (H1) and Livingston (L1) detectors observed the gravitational-wave event GW150914.

GW150914 was a watershed moment in astrophysics and gravitational-wave astronomy, marking the first direct detection of gravitational waves as predicted by Albert Einstein's general theory of relativity over a century earlier. This detection conclusively demonstrated that massive objects like black holes can generate ripples in space-time that propagate outward at the speed of light. The observed signal from GW150914 closely matched the theoretical predictions of general relativity for the merger of two black holes, thereby validating Einstein's theory in the extreme environment of black hole collisions, where gravitational effects are most pronounced.

Gravitational waves provide astronomers with a novel tool to observe the universe. Unlike

electromagnetic waves, which interact with matter and are often obscured, gravitational waves pass through the universe largely unimpeded. This unique property allows scientists to study violent events such as black hole mergers, neutron star collisions, and supernovae with unprecedented clarity and detail.

The detection of GW150914 revealed distinct phases in the gravitational-wave signal: an initial inspiral phase as the black holes spiraled closer together, a merger phase where they combined into a single black hole, and a final ring-down phase as the newly formed black hole settled into a stable state. The signal's frequency steadily increased from 35 to 150 Hz over approximately 0.2 seconds, reaching higher frequencies during the merger phase, indicating the tremendous energy released during the cataclysmic event.

Since GW150914, subsequent detections by LIGO and Virgo have further enhanced our understanding of the cosmos. Gravitational-wave astronomy now allows scientists to explore phenomena that were previously invisible, providing insights into the formation and evolution of black holes, the nature of neutron stars, and the dynamics of extreme gravitational environments.
This progression is guided by the anticipated gravitational-wave emissions from the gradual approach of two masses, denoted as m1 and m2. The transition to lower frequencies is distinguished by the chirp mass, a pivotal parameter that defines the gravitational-wave signature produced during the inspiral phase of such binaries.

$$\mathcal{M} = \frac{(m_1 m_2)^{3/5}}{(m_1 + m_2)^{1/5}} = \frac{c^3}{G}\left[\frac{5}{96}\pi^{-8/3} f^{-11/3}\dot{f}\right]^{3/5},$$

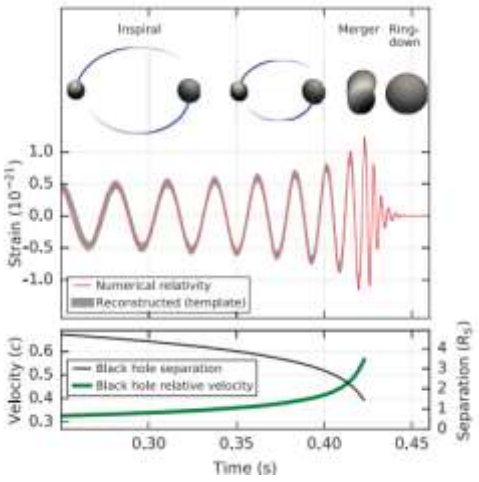

Figure 4.5.1.2 Top: Estimated amplitude of gravitational-wave strain from GW150914 as projected onto H1.

It seems like you're describing a figure or a panel that illustrates numerical relativity models depicting the merging horizons of black holes, possibly related to the GW150914 event. The inset images within this panel provide visual representations of these models, showcasing the process of black hole merger. In addition to these visualizations, the bottom panel of the figure presents data on the Keplerian effective separation between the black holes, measured in Schwarzschild radii (RS = 2GM/c^2), where G is the gravitational constant and c is the speed of light. This measurement offers crucial insights into the dynamics of the GW150914 event, detailing how the distance between the black holes evolved over time leading to their eventual merger. These visualizations and measurements are instrumental in understanding the gravitational-wave signal's evolution and the physical processes governing the inspiral and merger phases of the binary black hole system detected by LIGO. They provide a detailed view into the complex interactions and transformations occurring during such cataclysmic cosmic events.

CHAPTER 5

GRAVITATIONAL WAVE DETECTION USING QCNN AND CNN

5.1 INTRODUCTION

This study pioneers a methodological approach that integrates Quantum Convolutional Neural Networks (QCNN) alongside classical Convolutional Neural Networks (CNN) for the precise classification of gravitational wave signals. The dataset sourced from the G2Net gravitational wave dataset on Kaggle provides measurements from multiple detectors, meticulously sampled at high frequencies. Initial preprocessing involves standardizing and amalgamating time series data into spectrogram images, optimizing them for subsequent feature extraction processes. To harness the potential of quantum computing, QCNNs are introduced, employing quantum circuits to emulate convolutional operations. These circuits leverage specialized quantum gates to manipulate qubits, enabling computations that exploit quantum parallelism for enhanced efficiency and accuracy in signal classification tasks.

5.2 IMPLEMENTATION DESIGN

The methodology begins with data collection from the G2Net gravitational wave dataset on Kaggle, featuring measurements from multiple detectors sampled at high frequencies. Pre-processing involves normalization and combination of time series data into spectrogram images, optimizing them for feature extraction. The dataset is then split into training and validation sets to facilitate model development and evaluation.

For QCNN implementation, quantum circuits are designed to simulate convolutional operations, converting classical input data into quantum states for processing. These circuits utilize specialized quantum gates to manipulate qubits and perform computations that exploit quantum parallelism. Contrastingly, the CNN architecture follows traditional convolutional layers, integrating dropout regularization and dense layers for learning complex patterns from spectrogram inputs.

Model training involves optimizing parameters using the Adam optimizer and binary cross-entropy loss function, crucial for achieving high classification accuracy. Evaluation metrics such as confusion matrices and ROC curves assess model performance, comparing QCNNs and CNNs in terms of accuracy and computational efficiency.

By combining quantum computing advancements with classical neural network techniques, this study aims to push the boundaries of gravitational wave detection, demonstrating the potential of QCNNs to revolutionize real-time signal classification in astrophysical observations.

1. **DATA COLLECTION:** The dataset is sourced from G2Net gravitational wave dataset that is accessed on Kaggle.

```
array([[-2.29737815e-21, -2.14099891e-21, -1.71790095e-21, ...,
        -5.61538472e-21, -5.16897457e-21, -4.87839946e-21],
       [-8.46749671e-21, -8.34070032e-21, -8.27768338e-21, ...,
         3.89907386e-22,  5.46933090e-22,  5.58406202e-22],
       [-9.20862603e-22, -9.05587485e-22, -8.50850705e-22, ...,
         7.98082392e-22,  7.55659388e-22,  7.02043378e-22]])
```

	id	target
0	00000e74ad	1
1	00001f4945	0
2	0000661522	0
3	00007a006a	0
4	0000a38978	1
...	...	...
49995	16bbd5495a	0
49996	16bbd682aa	0
49997	16bbf24906	0
49998	16bc152384	0
49999	16bc3c0a51	1

50000 rows × 2 columns

Figure 5.2.1 Dataset

2. DATA INFORMATION: The dataset used in this project is sourced from the G2Net competition, which provides a comprehensive collection of simulated gravitational wave measurements. The dataset includes 50,000 training data samples carefully selected from an original dataset of 560,000 samples. These measurements originate from a network of three gravitational wave interferometers: LIGO Hanford, LIGO Livingston, and Virgo.

Each data sample in the dataset is stored in a numpy (npy) file format. These files contain three time series corresponding to measurements from each of the three detectors: LIGO Hanford,

LIGO Livingston, and Virgo. Each time series spans a duration of 2 seconds and is sampled at a frequency of 2,048 Hz. This high sampling rate allows for detailed capture of information related to both the gravitational wave signals and the background noise inherent in the detectors. The dataset is structured to include variations where each time series may either represent intrinsic detector noise or a combination of detector noise with a simulated gravitational wave signal.

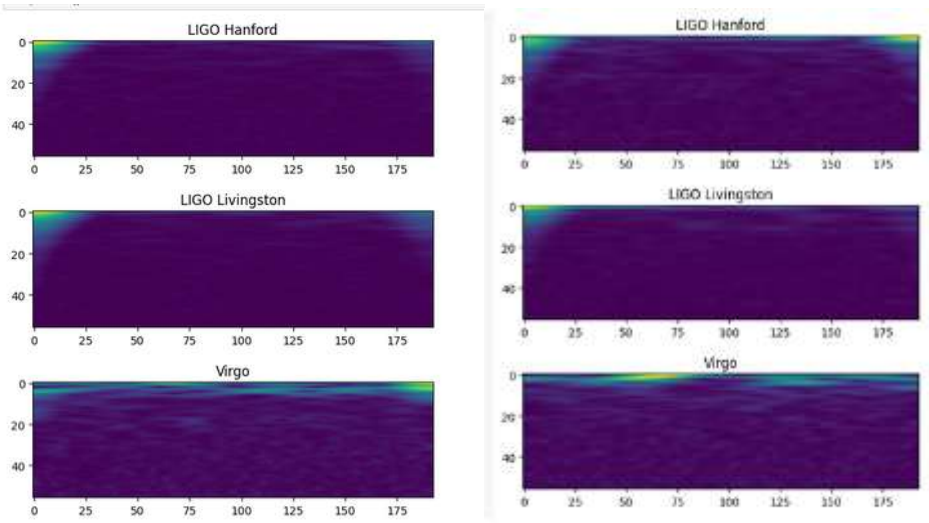

Figure 5.2.2 target 1 and target 0 respectively [spectrogram of each interferometer]

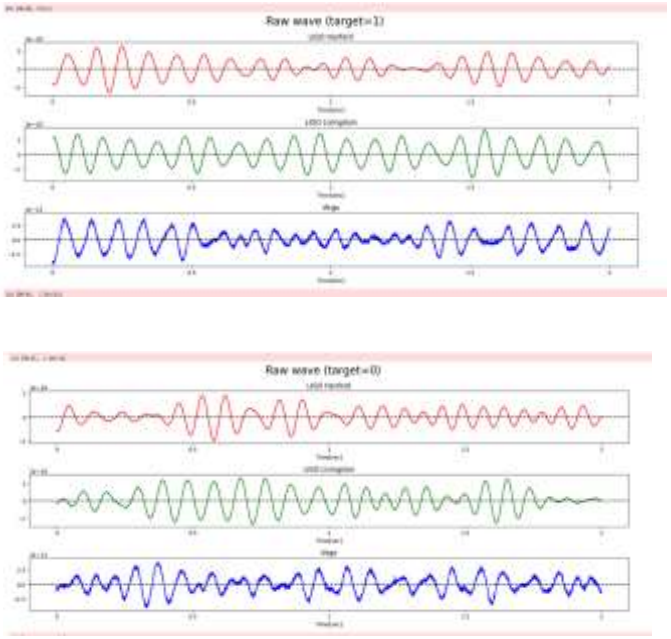

Figure 5.2.3 target 1 and target 0 respectively [waves of each interferometer]

3. FEATURE EXTRACTION: The process begins by loading the time series signal data from a numpy file, which typically contains measurements from each of the three detectors. To ensure consistent scaling across channels, each channel of the signal is normalized by dividing by its maximum value. This normalization step is essential for mitigating potential differences in signal amplitudes between detectors. Next, the normalized signals from all three channels are combined by horizontally stacking them together, resulting in a unified representation of the gravitational wave data. This consolidation of information enables the subsequent feature extraction process to leverage the collective insights provided by multiple detectors. The combined signal is then converted into a PyTorch tensor, facilitating further processing using PyTorch's computational capabilities. By applying the CQT transformation to the signal tensor, the method generates spectrogram images that encapsulate essential frequency-domain information, capturing variations in signal intensity across different frequency bands and time intervals. Finally, the spectrogram images with given input shape = (28, 96, 1) are converted to Tensor Flow tensors, to be utilized as input

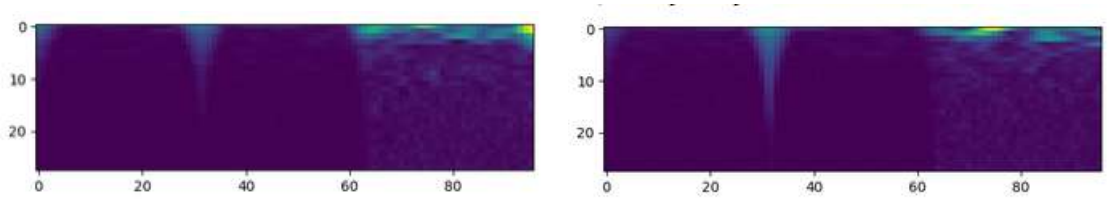

Figure 5.2.4 Target 1 and target 0 respectively [spectrogram images]

4. SPLITTING THE DATA: Data splitting is the process of dividing the dataset into several subsets for various uses. The dataset was split into training and validation. Data is utilized for validation in 5% of cases, and training in 95% of cases

5. CREATING QCNN MODEL

Define Parameters And Initialize The Layer: Set up the quantum convolutional layer by defining its parameters and initializing necessary components.

Filter Size: Determining the size of the convolutional filter is 2.

Depth: Specifying the number of filters (depth) in the convolutional layer is 3.

Activation Function: Choosing an activation function ReLU to apply after the convolution.

Quantum Circuit Construction: construction of a quantum circuit that performs convolution operations on input data encoded as quantum states. From the Cirq library to create a grid of qubits. Each qubit corresponds to a pixel in the filter size x filter size grid.

Classical Input Conversion: Classical data is encoded into quantum states using quantum gates. These gates rotate qubits to represent classical data in a quantum form.

Application of Quantum Gates: Constructs a layered quantum circuit using parameterized CZ (Controlled-Z) and CX (Controlled-X) gates. These gates interact with qubits in a hierarchical manner to simulate convolutional operations. Combines input circuit and QCNN_circuit to form a unified quantum circuit (full circuit) representing the entire operation of the quantum convolutional layer.

Building the Layer: Before processing data, the layer needs to be built to configure its parameters and internal states. Determines Input Dimensions: Extracts dimensions (width, height, channel) from the input data tensor. These dimensions determine how the convolutional filter slides over the input data.

Sets up Weight Matrix: Initializes the kernel parameter, which represents the quantum convolutional filters. These weights are adjusted during training to optimize the performance of the quantum convolutional layer.
Converts the constructed quantum circuit (full circuit) into a tensor (circuit tensor) using methods provided by Tensor Flow Quantum. This conversion facilitates efficient batch processing of input data through the quantum circuit.

Forward Pass: Defines how input data flows through the quantum convolutional layer during the forward pass.

Slicing and Transformation: Slices the input tensor into patches of size filter size x filter size. These patches are reshaped and organized for processing within the quantum circuit.

Batch Processing: Uses the circuit tensor to process each patch of input data in a batched manner. This involves applying the quantum circuit across multiple positions and channels (depth) within the input data

Activation and Output: Computes the output tensor by aggregating results from the quantum convolutional operations and applying an activation function (activation) to produce the final output of the layer

6. QUANTUM CONVOLUTION OPERATION:

Concatenates the input data (input data) with the kernel weights (controller) specific to the current depth level. This step prepares the inputs for processing through the quantum circuit.
Uses quantum computing principles (specifically, the expectation value computation) to evaluate the outcome of the quantum circuit given the concatenated inputs. This computation forms the basis of how convolutional operations are performed in a quantum context
Shapes and Structures: Reshapes and aggregates the quantum outputs to form the final output tensor for the current depth level (channel). This tensor represents the processed information after quantum convolution operations have been applied.

7. MODEL ARCHITECTURE DESIGN: Initialize a sequential model (qcnn_model) where layers are added sequentially. Introduce a custom QConv layer as the first layer in the sequential model.

Filter size: Specifies the size of the quantum convolution filter

Depth: Determines the number of output channels or filters.

Activation: Applies an activation function after convolution.
Input shape: Defines the shape of the input data expected by the model.

Flatten Layer: Convert 3D feature maps from the QConv layer into 1D feature vectors. Reshapes the output tensor from the QConv layer to prepare it for subsequent dense layers.

Dense Layer: Add a dense layer with specified number of neurons and activation function. Processes the flattened feature vector, applying a non-linear transformation (ReLU activation) to learn complex patterns in the data.

Dropout Layer: introduce dropout regularization to prevent over fitting.

Output Layer: Finalize the model with an output layer suitable for binary classification

```
Model: "sequential_1"
_________________________________________________________________
 Layer (type)                Output Shape              Param #
=================================================================
 q_conv_2 (QConv)            (None, 27, 95, 3)         18

 flatten_4 (Flatten)         (None, 7695)              0

 dense_8 (Dense)             (None, 32)                246272

 dropout_4 (Dropout)         (None, 32)                0

 dense_9 (Dense)             (None, 1)                 33

=================================================================
Total params: 246,323
Trainable params: 246,323
Non-trainable params: 0
```

Figure 5.2.5 Model QCNN summary

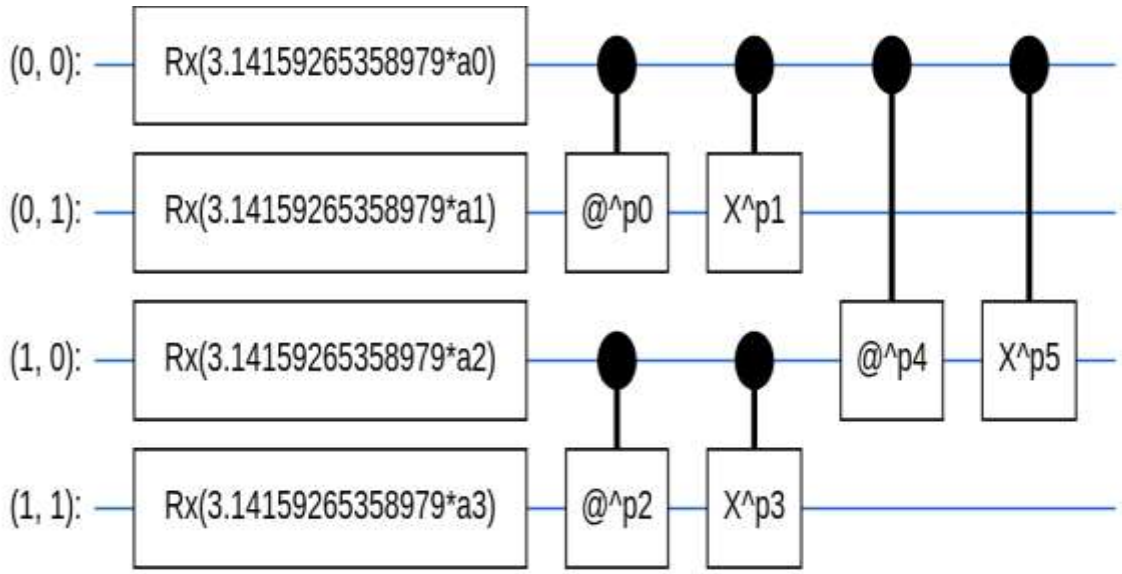

Figure 5.2.6 model Quantum circuit

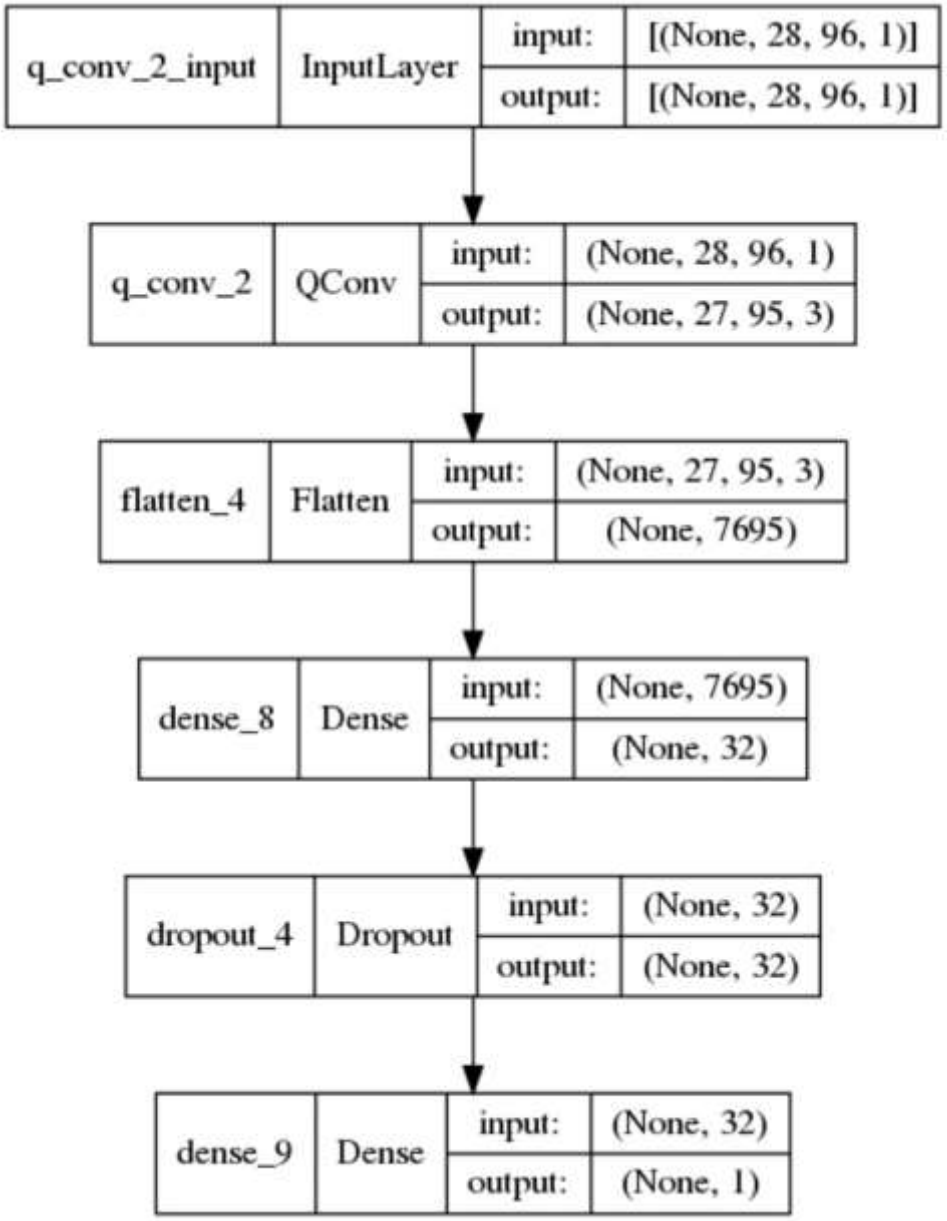

Figure 5.2.7 model QCNN architecture

8. MODEL COMPILATION: Configure the model for training. Specifies the optimization algorithm (Adam optimizer with a specific learning rate).

Loss: Defines the loss function (binary cross-entropy for binary classification).

Metrics: Evaluates model performance during training and validation

9. MODEL TRAINING: The model is trained using the model. Fit method. The data is taken as batches on undergoing process.

10. MODEL EVALUATION: For the performance evaluation, various performance measures such as accuracy, confusion matrix, and ROC curve of the model were calculated. Detailed performance evaluation is done in Chapter 5.

11. CREATING CNN MODEL

Sequential Model Initialization: Initialize a sequential model (model_cnn) where layers are added sequentially.

12. MODEL ARCHITECTURE DESIGN:

Adding Conv2D Layer: Introduce a 2D convolutional layer as the first layer in the sequential model.

Filters: 3, specifying the number of output filters in the Convolution.

Kernel size: 3, indicating the height and width of the 2D Convolution window.

Input shape: Specifies the shape of the input data expected by the model.

Activation: Uses ReLU activation to introduce non-linearity.

Padding: 'same', meaning the output has the same spatial dimensions as the input.

Flatten Layer: Convert 3D feature maps from the Conv2D layer into 1D feature vectors. Reshapes the output tensor from the Conv2D layer to prepare it for subsequent dense layers.

Dense Layer: Add a dense layer with specified number of neurons and activation function. Processes the flattened feature vector, applying a non-linear transformation (ReLU activation) to learn complex patterns in the data

Dropout Layer: Introduce dropout regularization to prevent over fitting. Randomly drops a fraction of neurons (50% in this case) during training to improve model generalization

Output Layer: Finalize the model with an output layer suitable for binary classification task. Applies a sigmoid activation function to produce a probability score between 0 and 1, indicating the likelihood of the input belonging to a particular class.

```
Model: "CNN_model"
_________________________________________________________________
 Layer (type)                Output Shape              Param #
=================================================================
 conv2d_2 (Conv2D)           (None, 28, 96, 3)         30

 flatten_2 (Flatten)         (None, 8064)              0

 dense_4 (Dense)             (None, 32)                258080

 dropout_2 (Dropout)         (None, 32)                0

 dense_5 (Dense)             (None, 1)                 33

=================================================================
Total params: 258,143
Trainable params: 258,143
Non-trainable params: 0
_________________________________________________________________
```

Figure 5.2.8 model CNN summary

13. MODEL COMPILATION: Configure the model for training

Optimizer: Specifies the optimization algorithm (Adam optimizer with a specific learning rate).

Loss: Defines the loss function (binary cross-entropy for binary classification).

Metrics: Evaluates model performance during training and validation

14. MODEL TRAINING: The model is trained using the model. Fit method. The data is taken as batches on undergoing process.

15. MODEL EVALUATION: For the performance evaluation, various performance measures such as accuracy, confusion matrix, and ROC curve of the model were calculated. Detailed performance evaluation is done in 5.3

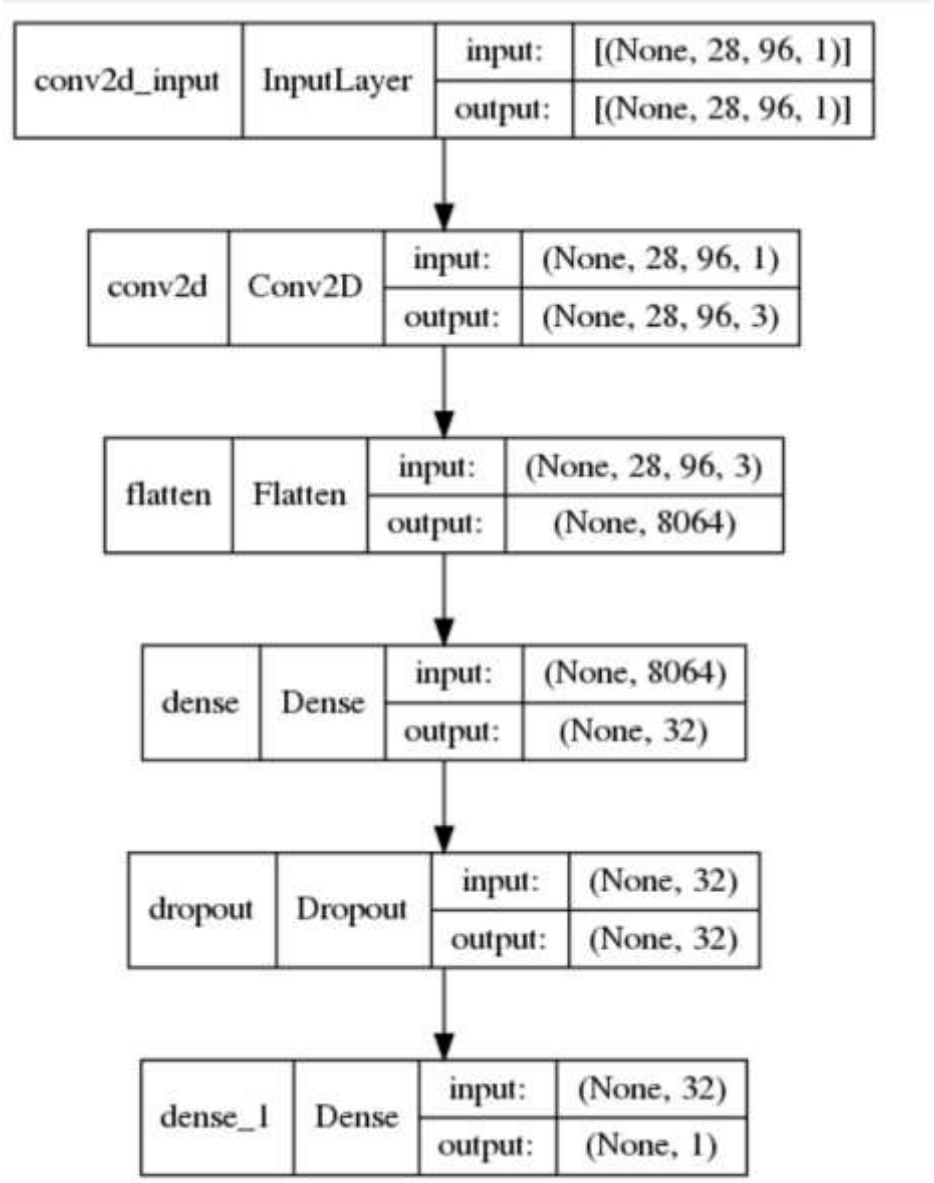

Figure 5.2.9 model CNN architecture

5.3 EXPERIMENTAL RESULT

CONFUSION MATRIX

To evaluate how well the QCNN (Quantum Convolutional Neural Network) and CNN (Convolutional Neural Network) models classify gravitational waves, we analyze parameters

derived from the confusion matrix. This matrix, depicted in figure 17, is a square NxN matrix used to assess the accuracy of classification models by detailing predictions across different classes

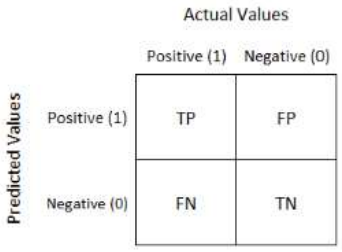

Figure 2: confusion matrix

Figure 5.3.1 confusion matrix

Accuracy: Accuracy is a measure of how well a model performs on a specific task

Accuracy = (TP + TN) / (TP + TN + FP + FN)

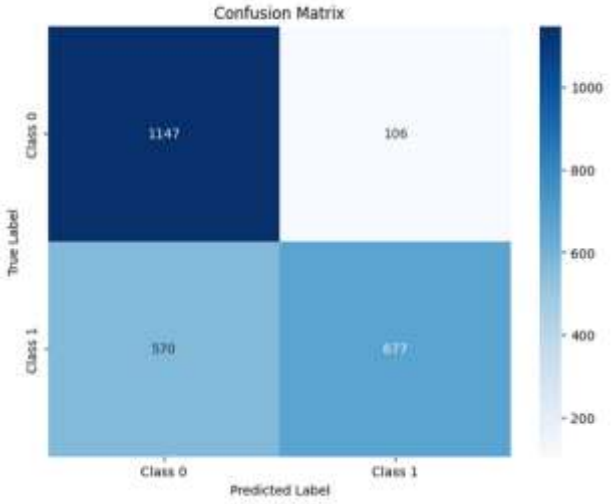

Figure 5.3.2 confusion matrix of QCNN

The QCNN model correctly predicted that 1147 true positives and it also correctly predicted that 677 true negatives. The model incorrectly predicted those 106 false positives and 570 false negatives

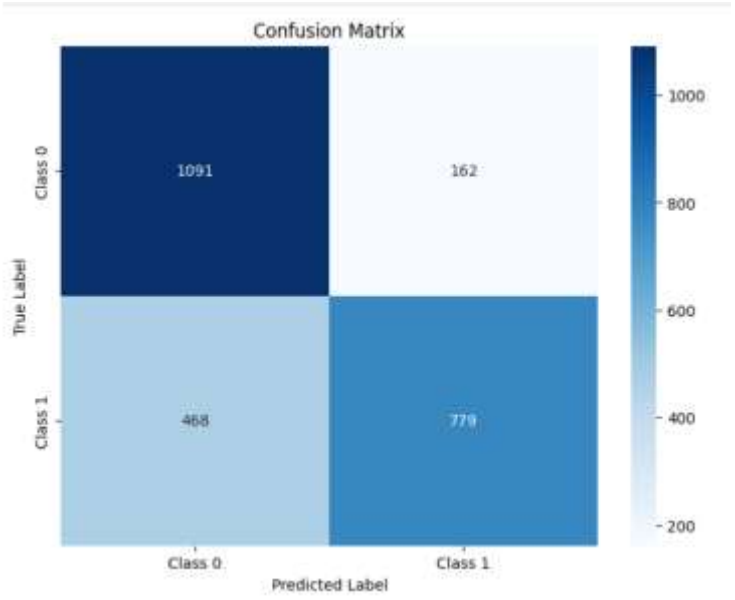

Figure 5.3.3 confusion matrix of CNN

The CNN model correctly predicted that 1091 true positives and it also correctly predicted that 779 true negatives. The model incorrectly predicted that 162 false positives and 468 false negatives

ACCURACY CURVE AND LOSS CURVE

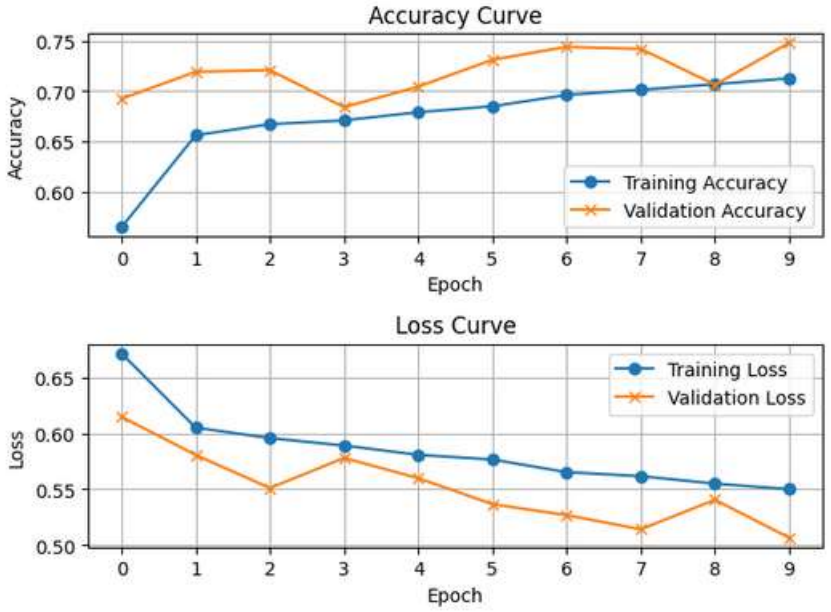

Figure 5.3.4 Accuracy curve and loss curve of QCNN

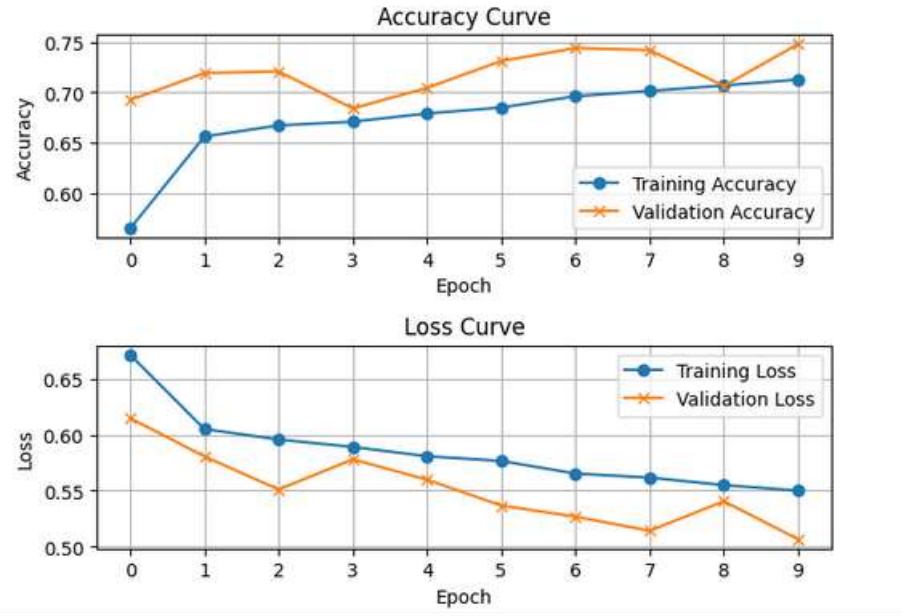

Figure 5.3.5 Accuracy curve and loss curve of the model CNN

ROC CURVE

The ROC (Receiver Operating Characteristic) curve is a visual representation that evaluates the performance of a binary classification model. It plots the trade-off between the true positive rate (TPR) and the false positive rate (FPR) across different threshold settings used to classify observations as positive or negative.

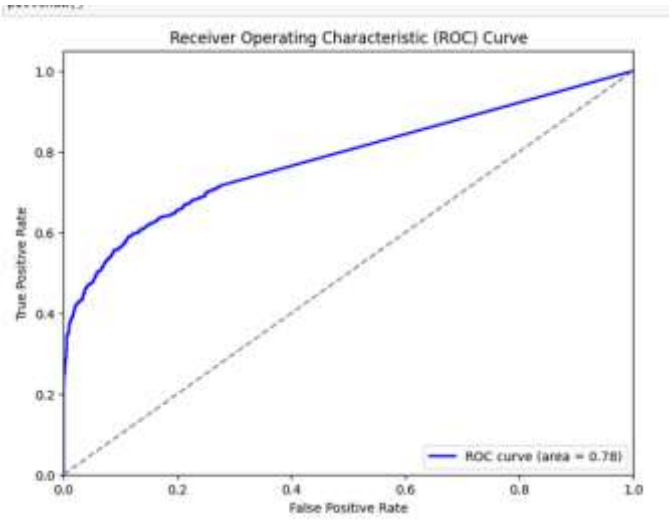

Figure 5.3.6 ROC CURVE of QCNN

The QCNN model performs over 0.5 threshold value. The AUC ROC measures the overall performance that is 0.78

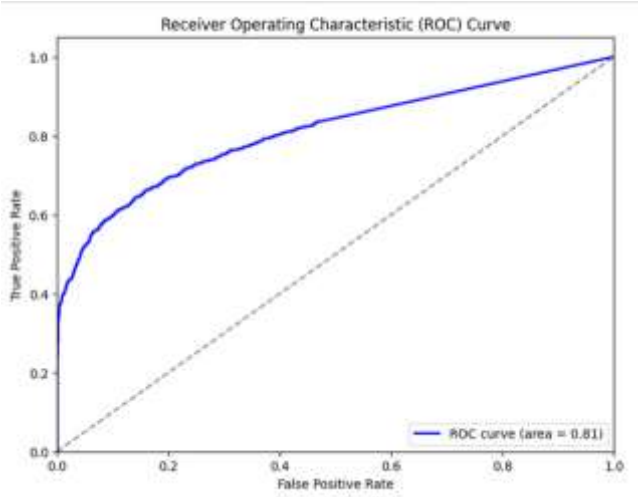

Figure 5.3.7 ROC CURVE of CNN

The CNN model performs over 0.5 threshold value. The AUC ROC measures the overall performance that is 0.81

5.4 CONCLUSION

The QCNN model achieved a performance where it correctly identified 1147 true positives and 677 true negatives, with 106 false positives and 570 false negatives. This indicates a balanced performance in distinguishing between positive and negative instances. Comparatively, the CNN model, while also effective, showed slightly different performance metrics with 1091 true positives and 779 true negatives, along with 162 false positives and 468 false negatives. The CNN model demonstrated a marginally higher overall performance with an AUC ROC of 0.81 compared to the QCNN's AUC ROC of 0.78, while conventional Convolutional Neural Networks (CNNs) achieved marginally higher accuracy metrics in this specific study, the QCNN's quantum-inspired architecture holds transformative potential. By leveraging quantum computation's unique properties, QCNNs open new avenues for precise analysis of cosmic events.

CHAPTER 6

GRAVITATIONAL WAVE DETECTION BY ADDING THERMAL NOISE

6.1 INTRODUCTION

Thermal noise, known scientifically as Johnson-Nyquist noise, is a fundamental source of random fluctuations in electronic systems arising from the thermal motion of electrons within conductors. This noise exhibits a Gaussian distribution across all frequencies, commonly referred to as "white noise," with its intensity directly linked to temperature through Boltzmann's constant. Understanding and managing thermal noise are crucial in various fields of science and engineering where signal fidelity is paramount.

This study delves into the characterization and mitigation of thermal noise in electronic signals. Initially, the research quantifies the power of thermal noise and explores its simulation by adding it to original signals across different Signal-to-Noise Ratio (SNR) levels. Visualizations using Constant-Q Transform (CQT) spectrograms provide a detailed analysis of how thermal noise affects frequency-domain characteristics and temporal variations in signal amplitude.

To mitigate the impact of thermal noise, the study investigates two prominent noise reduction techniques: Wiener filtering and Bayesian inference. These methods are evaluated based on their ability to enhance the Signal-to-Noise Ratio (SNR) through rigorous computational analysis and comparative spectrogram visualizations. The performance of these techniques is further assessed using advanced machine learning models such as Quantum Convolutional Neural Networks (QCNN) and Convolutional Neural Networks (CNN), highlighting their effectiveness in improving signal clarity amidst noise interference.

6.2 IMPLEMENTATION DESIGN

The study commences with an exploration of thermal noise, also known as Johnson-Nyquist noise, which pervades electronic systems as a consequence of the random thermal motion of electrons within conductors. This noise exhibits a Gaussian distribution across all frequencies, commonly referred to as "white-noise” and its intensity is directly proportional to temperature, as elucidated by Boltzmann's constant. By quantifying the noise power, the study simulates its

addition to original signals across various Signal-to-Noise Ratio (SNR) levels. Visualizing the influence of this noise on signal integrity is facilitated through Constant-Q Transform (CQT) spectrograms, offering insights into frequency-domain characteristics and temporal amplitude fluctuations.

The methodology proceeds with the application of two distinct noise reduction techniques: Wiener filtering and Bayesian inference. Wiener filtering operates in the frequency domain to enhance the signal-to-noise ratio by minimizing the mean square error between original and noisy signals. In contrast, Bayesian inference leverages known statistical properties of noise to estimate and subtract noise components from the signal. Evaluation metrics encompass SNR calculations, comparative visualizations of noisy and cleaned signals using spectrograms, and performance assessments employing Quantum Convolutional Neural Networks (QCNN) and Convolutional Neural Networks (CNN). These analyses collectively underscore the efficacy of the denoising strategies.

The primary objective of this study is to advance understanding of noise mitigation strategies essential in applications where signal fidelity is paramount. By evaluating the performance improvements in QCNN and CNN models following noise reduction.

1) GENERATING THERMAL NOISE:

Thermal noise, or Johnson-Nyquist noise, is a form of random electrical noise caused by the natural movement of electrons within a conductor due to their thermal energy. This phenomenon is ubiquitous in electronic circuits and arises because of the thermal motion of charge carriers, primarily electrons. As the conductor's temperature increases, so does the amplitude of this noise, which manifests as random fluctuations in voltage and current. These fluctuations follow a Gaussian distribution, centered around zero, meaning the noise varies randomly in a manner typical of a normal distribution curve.

The power spectral density of thermal noise is uniform across all frequencies, exhibiting equal intensity at every frequency—a characteristic referred to as white noise. The magnitude of thermal noise power depends directly on the temperature of the conductor and the bandwidth over which it is measured. Specifically, the mean-square noise voltage across a resistor R over a bandwidth B at temperature Tis given by:

$$V_n^2 = 4kTRB$$

Where k is Boltzmann's constant.

For a resistor at room temperature (T≈300K), this formula can be used to calculate the noise voltage

Signal Power Calculation: The average power of the original signal is calculated. Signal power is a measure of the signal's strength and is computed as the mean of the squared signal values. : Different SNR levels are set to observe the impact of varying noise intensities.

$$\text{Signal Power} = \frac{1}{N}\sum_{i-1}^{N} x_i^2$$

Noise Power Calculation: The level of noise power required is determined by the desired Signal-to-Noise Ratio (SNR), which serves as a metric for assessing the quality of a signal. SNR quantifies the ratio between the power of the signal of interest and the power of accompanying noise. A higher SNR signifies a clearer signal with less interference from noise, thereby indicating better signal quality.

$$\text{noise\_power} = \frac{\text{signal\_power}}{10^{(\text{snr\_db}/10)}}$$

Noise Generation: Thermal noise is simulated using a Rayleigh distribution, which is scaled to match the calculated noise power. This ensures that the noise exhibits the correct intensity relative to the original signal. The Rayleigh distribution is appropriate for modeling thermal noise because it characterizes random processes with non-negative values and aligns well with the statistical properties of noise in electronic systems.

2. ADDING NOISE TO THE SIGNAL: The generated thermal noise is added to the original signal. Adding different levels of noise (0 dB, 10 dB, 20 dB, 30 dB) .The addition of noise are done by simple element-wise addition of the noise array to the signal array. This creates a noisy version of the original signal

3. COMPUTING THE RESULTING SNR: After adding the noise, the resulting SNR is

computed to quantify the impact of the noise. The resulting SNR gives a measure of the quality of the noisy signal compared to the original signal. The resulting SNR is calculated by comparing the power of the original signal to the power of the noisy signal, which includes the added noise.

$$\text{SNR} = 10 \log_{10} \left(\frac{\text{Signal Power}}{\text{Noise Power}} \right)$$

4. VISUALIZING THE NOISY SIGNAL: The noisy signal is visualized to analyze the impact of the added noise

Frequency Representation: The noisy signal is transformed using the Constant-Q Transform (CQT) and displayed as a 2D image. This representation shows how different frequency components of the signal are affected by the noise.

Waveform Plot: The waveform of the added noise is plotted to show its amplitude variations over time. This plot helps in understanding the nature of the noise and its temporal characteristics

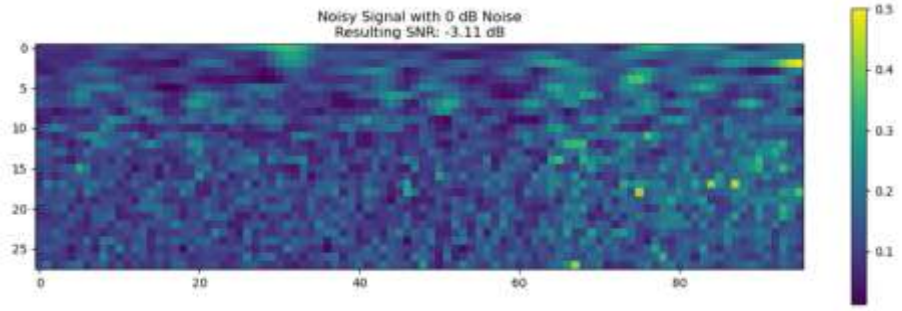

Figure 6.2.1 noisy signal with 0 dB noise

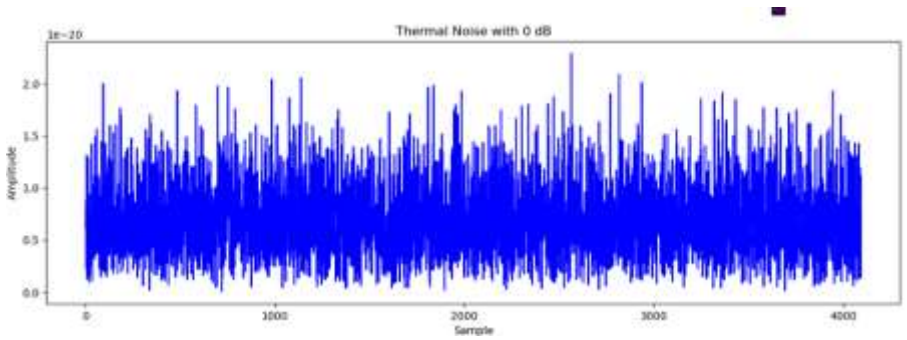

Figure 6.2.2 thermal noise with 0dB

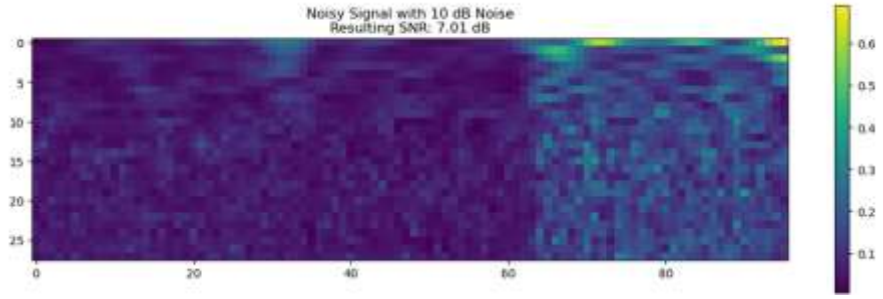

Figure 6.2.3 noisy signal with 10 dB noise

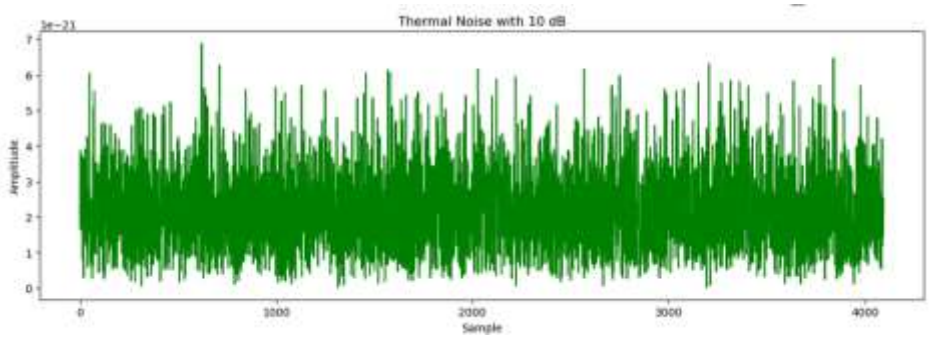

Figure 6.2.4 thermal noise with 10dB

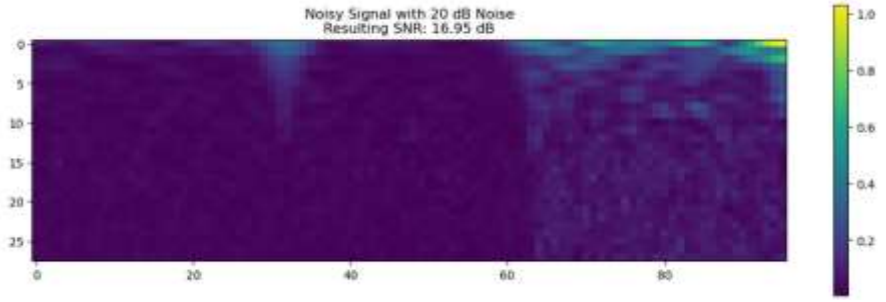

Figure 6.2.5 noisy signal with 20 dB noise

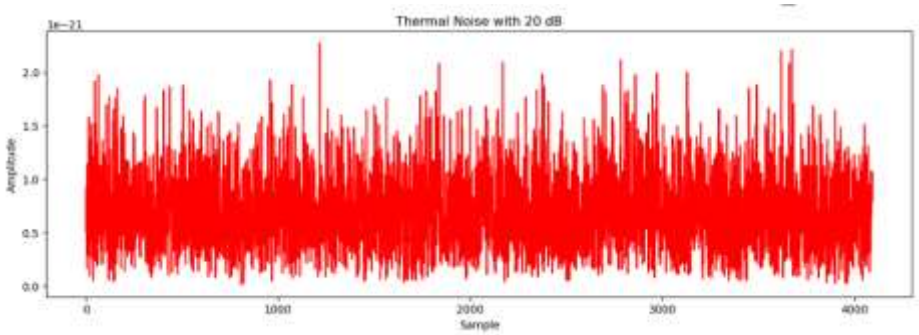

Figure 6.2.6 thermal noise with 20dB

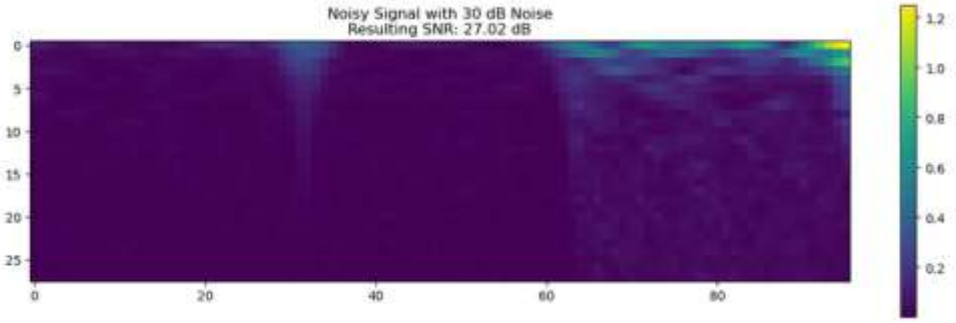

Figure 6.2.7 noisy signal with 30 dB noise

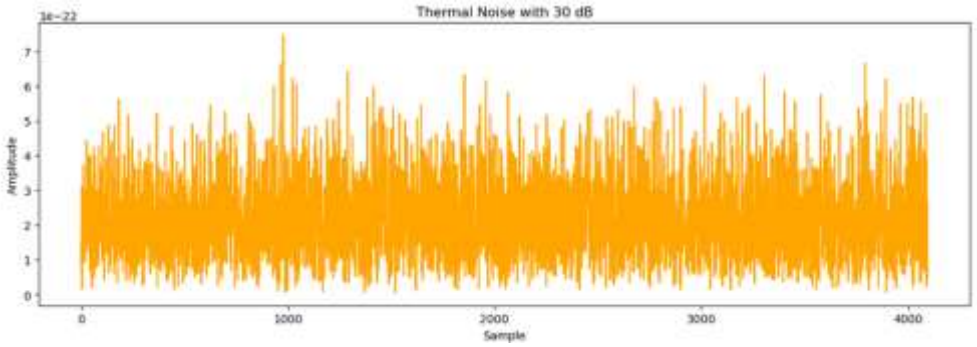

Figure 6.2.8 thermal noise with 30dB

5. REMOVING NOISE USING WIENER FILTERING: The main objective of Wiener filtering is to diminish noise in a signal while retaining essential signal characteristics. This method involves applying a Wiener filter individually to each channel of a noisy signal. The filter achieves noise reduction by minimizing the mean square error (MSE) between the estimated signal and the original signal.

In frequency domain terms, the transfer function H (f) of the Wiener filter is determined. This function is computed to optimize the filter coefficients, ensuring they minimize the MSE between the estimated and actual signals. The Wiener filter operates by leveraging statistical properties of both the noise and the desired signal to enhance signal clarity amidst noise interference, making it a valuable tool in signal processing applications.

$$H(f) = \frac{S_x(f)}{S_x(f) + S_n(f)}$$

Where Sx (f) is the power spectral density (PSD) of the signal and Sn(f) is the PSD of the noise.

6. COMPUTING SNR AFTER NOISE REMOVAL: Signal-to-Noise Ratio (SNR) serves as a

metric to gauge the relative strength of the desired signal against background noise. Following the application of a Wiener filter to attenuate noise from the signal, the SNR is recalculated to assess the effectiveness of the noise reduction process. This recalculated SNR helps evaluate the extent to which the noise reduction procedure has enhanced the quality and clarity of the signal.

Signal Power: Calculate the power of the original (clean) signal

$$\text{Signal Power} = \frac{1}{N}\sum_{i-1}^{N} x_i^2$$

Where xi is the samples of the original signal and N is the number of samples.

Noise Power: Calculate the power of the noise in the cleaned signal.

$$\text{Noise Power} = \frac{1}{N}\sum_{i-1}^{N} (y_i - x_i)^2$$

Where yi are the samples of the cleaned signal.

SNR Calculation: Compute the SNR in decibels (dB).

$$\text{SNR} = 10\log_{10}\left(\frac{\text{Signal Power}}{\text{Noise Power}}\right)$$

A higher SNR indicates a better quality signal with less noise.

7. **VISUALIZING CLEANED SIGNAL:** visualizing the signals after noise removed

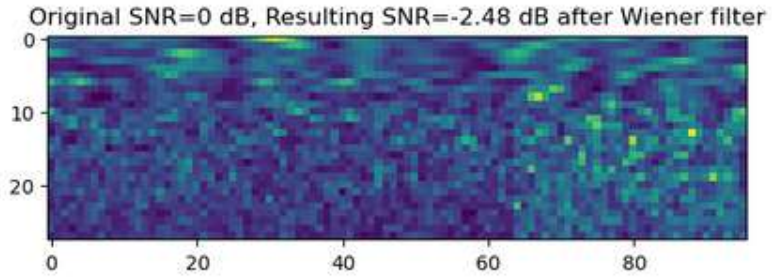

Figure 6.2.9 after removing noise 0 dB using wiener filter

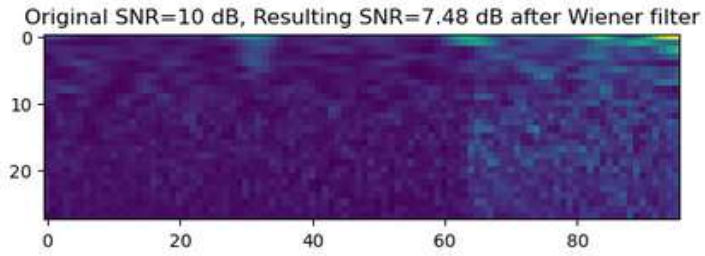

Figure 6.2.10 after removing noise 10 dB using wiener filter

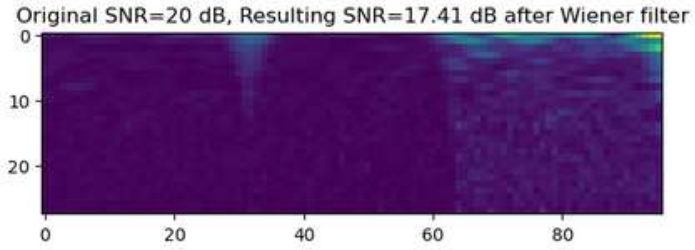

Figure 6.2.11 after removing noise 20 dB using wiener filter

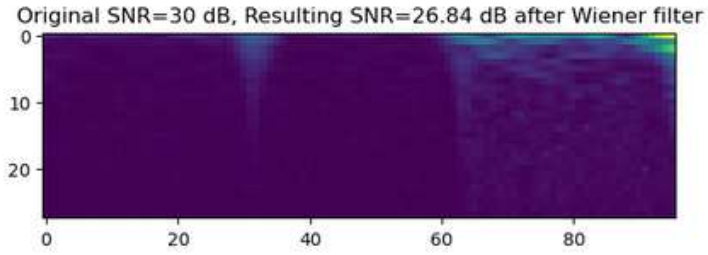

Figure 6.2.12 after removing noise 30 dB using wiener filter

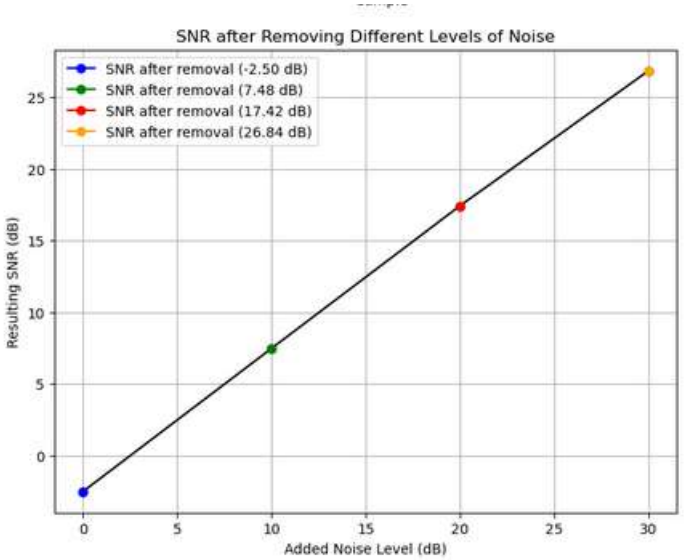

Figure 6.2.13 SNR after removing different levels of noise using wiener filter

8. NOISE REMOVAL USING BAYESIAN INFERENCE:

Noise Mean Calculation: First, the mean of the noise is calculated. This involves taking the average value of the noise, which represents the central tendency of the noise values.

Signal Estimation: The clean signal is then estimated by subtracting this mean noise value from the noisy signal. Mathematically, this is expressed as:

$$\text{clean\_signal} = \text{noisy\_signal} - \text{mean}(\text{noise})$$

This method assumes that the noise added to the signal has a known statistical property, specifically its mean. By subtracting this mean, the assumption is that the primary contribution of the noise to the signal can be mitigated, thus enhancing the original signal's quality.

9. COMPUTING SNR AFTER NOISE REMOVAL:

Signal-to-Noise Ratio (SNR) is a metric used to quantify the strength of a desired signal relative to the background noise. Following the application of Bayesian inference to suppress noise from the signal, the SNR is recalculated to assess the effectiveness of this noise reduction technique. This updated SNR measurement serves as an evaluation of how effectively the noise removal process has enhanced the quality and clarity of the signal. A higher SNR after Bayesian inference indicates successful noise reduction, leading to improved signal fidelity and usability for subsequent analysis or applications.

10. VISUALIZATION AND ANALYSIS:

For each Signal-to-Noise Ratio (SNR) level (0 dB, 10 dB, 20 dB, 30 dB):

Visualize the cleaned signal transformed into an image using the CQT transformation. The image is displayed with labels showing the original SNR and the resulting SNR after noise removal using Bayesian inference.

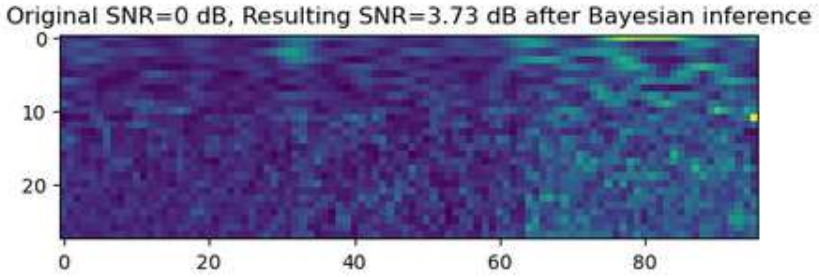

Figure 6.2.14 after removing noise 0 dB using Bayesian inference

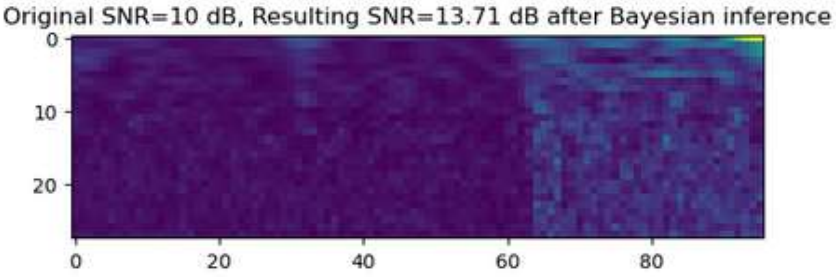

Figure 6.2.15 after removing noise 10 dB using Bayesian inference

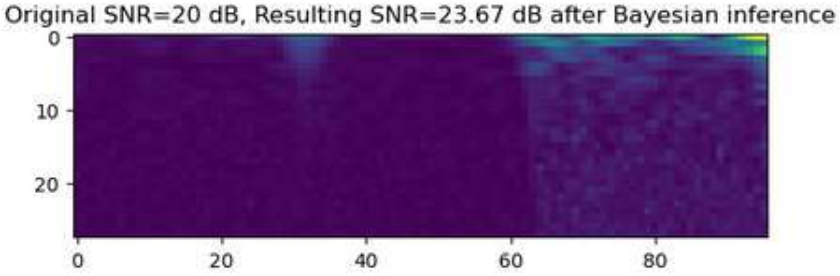

Figure 6.2.16 after removing noise 20 dB using Bayesian inference

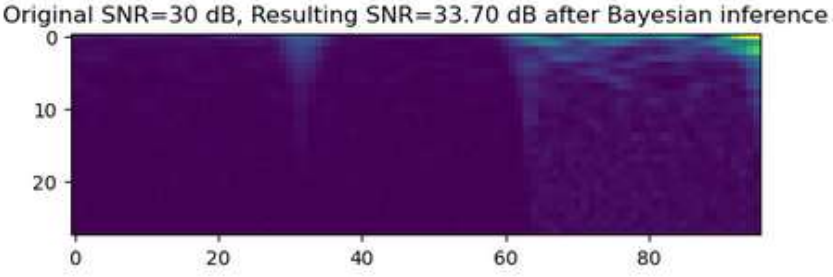

Figure 6.2.17 after removing noise 30 dB using Bayesian inference

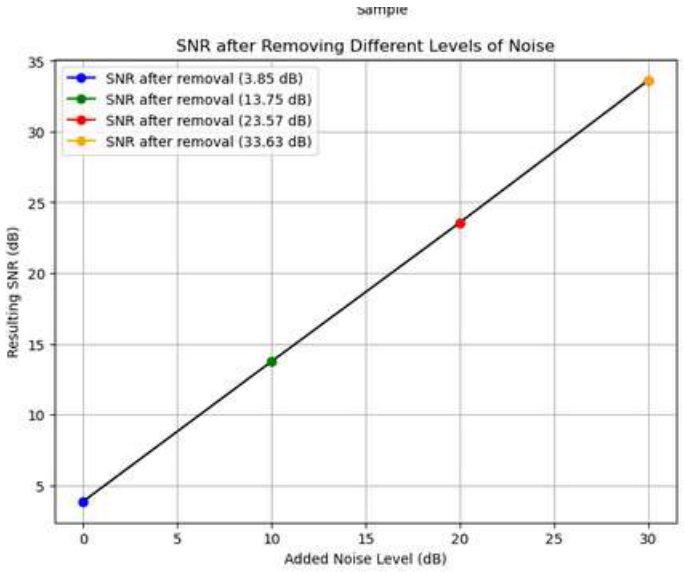

Figure 6.2.18 SNR after removing different levels of noise using Bayesian inference

After generating thermal noise at these specified SNR levels, we applied Bayesian inference and wiener filter to remove the noise and then computed the resulting SNRs to assess the quality of the cleaned signals. Our findings indicate that the signal with 30 dB noise level consistently produced a higher resulting SNR after noise removal, indicating a clearer and higher quality signal compared to the other levels.

11. MODEL TRAINING AND EVALUATION: The QCNN and CNN model is trained using data with 30 dB thermal noise added.

12. MODEL PERFORMANCE EVALUATION:

Model Accuracy: Model accuracy measures how often the model correctly predicts instances across all evaluations. It offers a straightforward assessment of how well the model performs overall.

Confusion Matrix: A confusion matrix is a structured table that provides detailed insights into the classifier's performance. It categorizes predictions into four outcomes: true positives (correctly predicted positives), true negatives (correctly predicted negatives), false positives (incorrectly predicted as positives), and false negatives (incorrectly predicted as negatives). This matrix is essential for identifying where the classifier excels and where it may struggle across different classes.

ROC Curve (Receiver Operating Characteristic Curve): The ROC curve assesses the model's ability to distinguish between positive and negative classes by varying classification thresholds. It plots the true positive rate (TPR) against the false positive rate (FPR). A higher area under the ROC curve (AUC-ROC) indicates better discrimination capability of the model. An ideal classifier achieves an AUC-ROC of 1, indicating perfect discrimination between classes.

13. COMPARING THE QCNN MODEL BEFORE AND AFTER ADDING NOISE: comparison between the QCNN model's performance before and after adding 30 dB thermal noise by training and validation accuracy curve

14. COMPARING THE CNN MODEL BEFORE AND AFTER ADDING NOISE: comparison between the CNN model's performance before and after adding 30 dB thermal noise by training and validation accuracy curve

15. REMOVING NOISE USING WIENER FILTERING: Removing noise from QCNN and CNN model using a Wiener filter also reveals significant impacts on its accuracy, confusion matrix, and overall classification ability

16. REMOVING NOISE USING BAYESIAN INFERENCE: Removing noise from QCNN and CNN using Bayesian inference also reveals significant impacts on its accuracy, confusion matrix, and overall classification ability

17. QCNN PERFORMANCE ANALYSIS: The final graph shows that the Wiener filter and Bayesian inference in terms of both training and validation accuracy. The purpose of this graph is to asses which denoising method was best for noise removal from this model

18. CNN PERFORMANCE ANALYSIS: The final graph shows that the Wiener filter and Bayesian inference in terms of both training and validation accuracy. The purpose of this graph is to asses which denoising method was best for noise removal from this model

6.3 EXPERIMENTAL RESULT

6.3.1 ADDING THERMAL NOISE

CONFUSION MATRIX

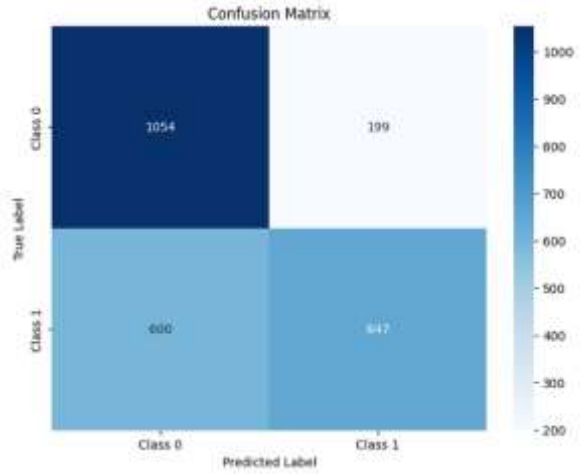

Figure 6.3.1.1 confusion matrix of QCNN while adding thermal noise

The QCNN model correctly predicted that 1054 true positives and it also correctly predicted that 647 true negatives. The model incorrectly predicted those 199 false positives and 600 false negatives

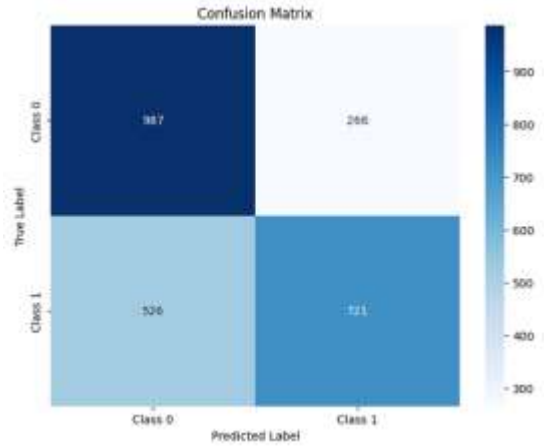

Figure 6.3.1.2 confusion matrix of CNN while adding thermal noise

The CNN model correctly predicted that 984 true positives and it also correctly predicted that 721 true negatives .the model incorrectly predicted those 266 false positives and 526 false negatives

ACCURACY CURVE AND LOSS CURVE

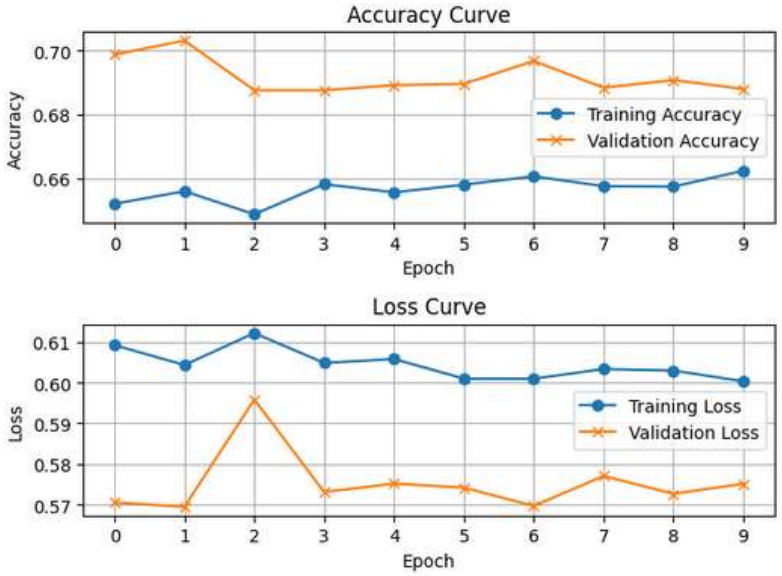

Figure 6.3.1.3 Accuracy curve and loss curve of QCNN while adding thermal noise

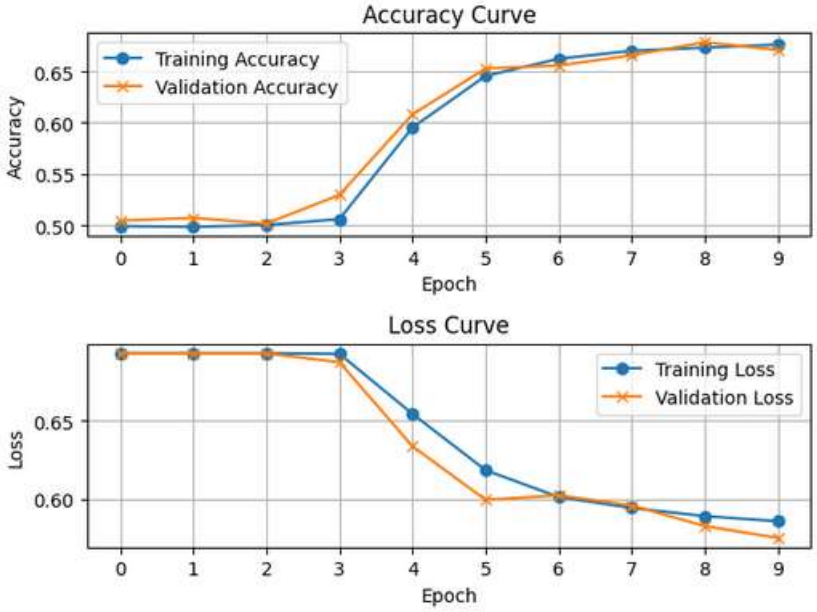

Figure 6.3.1.4 Accuracy curve and loss curve of CNN while adding thermal noise

ROC CURVE

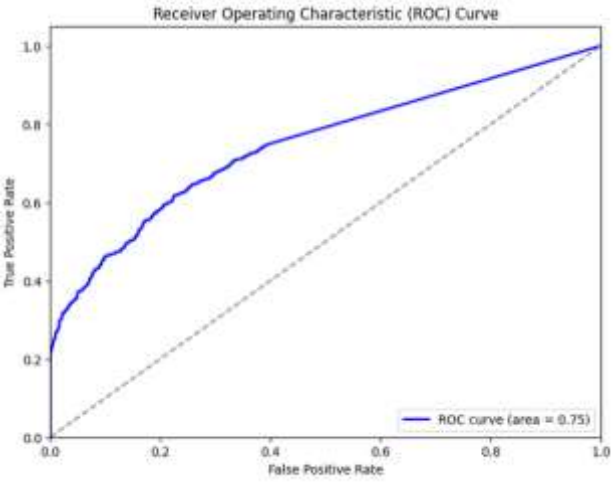

Figure 6.3.1.5 ROC CURVE OF QCNN

The QCNN model performs over 0.5 threshold value. The AUC ROC measures the overall performance that is 0.75

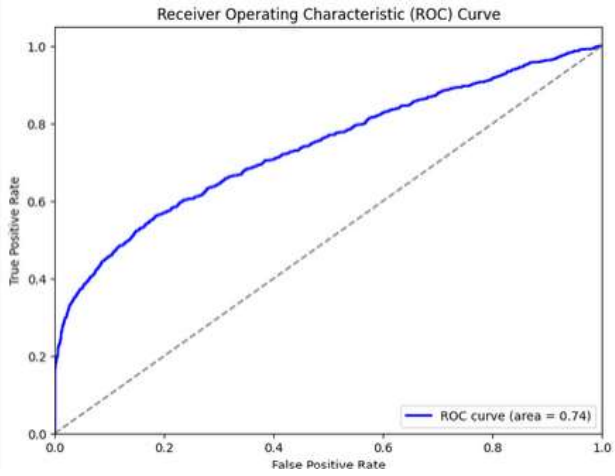

Figure 6.3.1.6 ROC CURVE OF CNN

The QCNN model performs over 0.5 threshold value. The AUC ROC measures the overall performance that is 0.74

6.3.2 REMOVING THERMAL NOISE USING WIENER FILTER

CONFUSION MATRIX

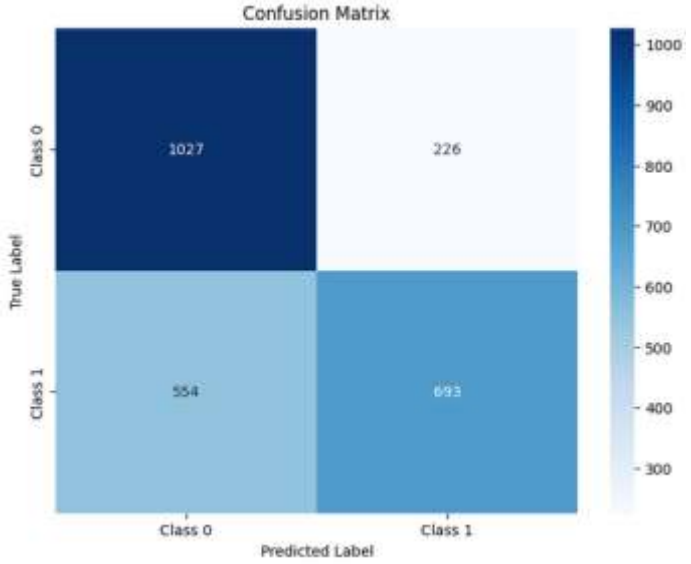

Figure 6.3.2.1 confusion matrix of QCNN while removing thermal noise using wiener filter

The QCNN model correctly predicted that 1027 true positives and it also correctly predicted that 693 true negatives .the model incorrectly predicted those 226 false positives and 554 false negatives

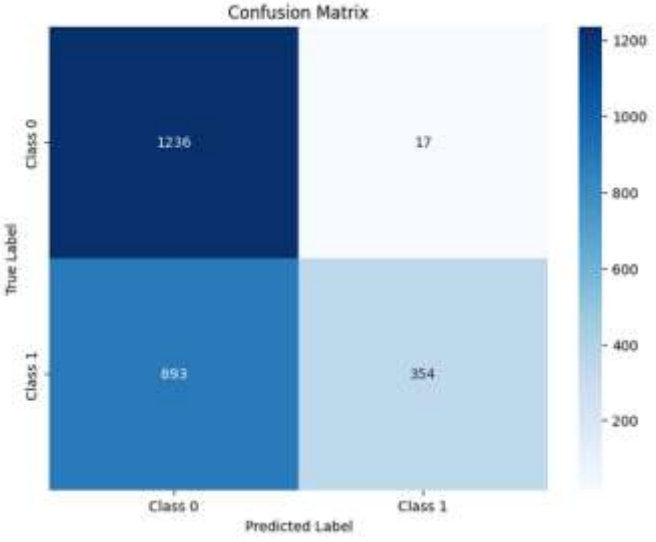

Figure 6.3.2.2 confusion matrix of CNN while removing thermal noise using wiener filter

The CNN model correctly predicted that 1236 true positives and it also correctly predicted that 354 true negatives .the model incorrectly predicted those 17 false positives and 893 false negatives

ACCURACY CURVE AND LOSS CURVE

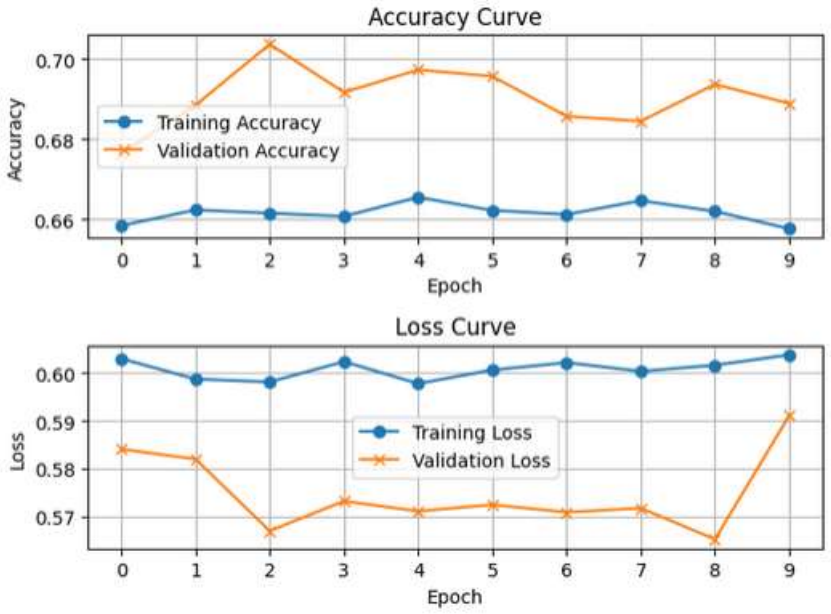

Figure 6.3.2.3 accuracy curve and loss curve of QCNN while removing thermal noise

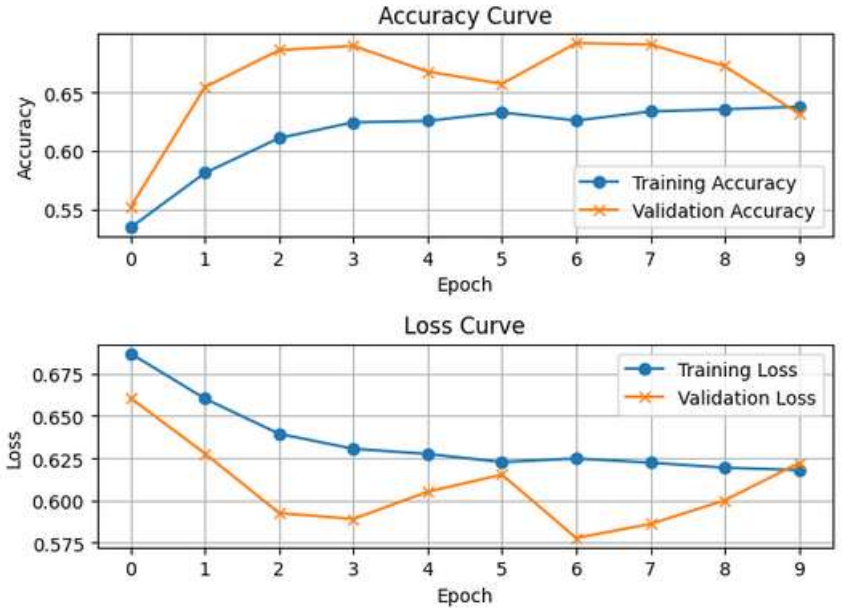

Figure 6.3.2.4 accuracy curve and loss curve of CNN while removing thermal noise

ROC CURVE

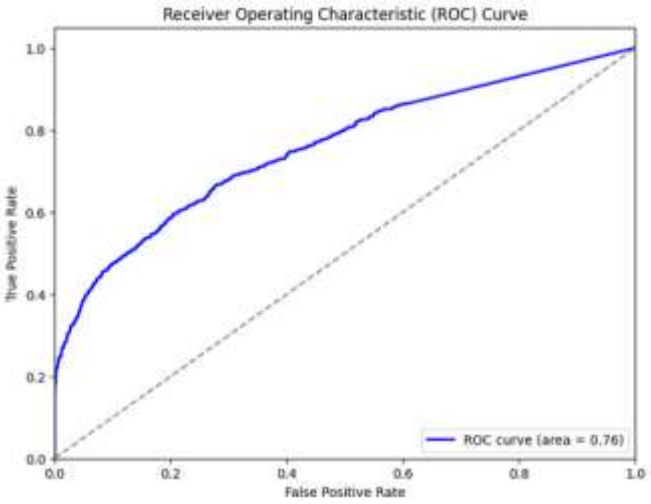

Figure 6.3.2.5 ROC CURVE OF QCNN while removing thermal noise

The QCNN model performs over 0.5 threshold value. The AUC ROC measures the overall performance that is 0.76

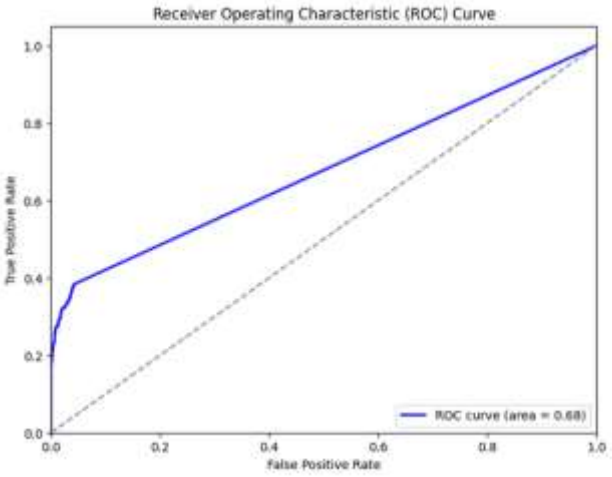

Figure 6.3.2.6 ROC CURVE OF CNN while removing thermal noise

The CNN model performs over 0.5 threshold value. The AUC ROC measures the overall performance that is 0.68

6.3.3 REMOVING THERMAL NOISE USING BAYESIAN INFERENCE

CONFUSION MATRIX

Figure 6.3.3.1 QCNN while removing thermal noise

The QCNN model correctly predicted that 1059 true positives and it also correctly predicted that 681 true negatives .the model incorrectly predicted those 194 false positives and 566 false negatives

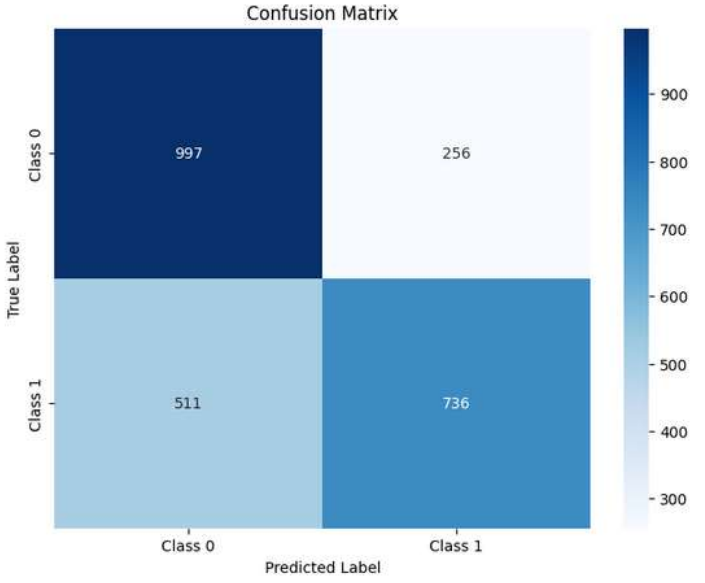

Figure 6.3.3.2 CNN while removing thermal noise

The CNN model correctly predicted that 997 true positives and it also correctly predicted that 736 true negatives .the model incorrectly predicted those 256 false positives and 511 false negatives

ACCURACY CURVE AND LOSS CURVE

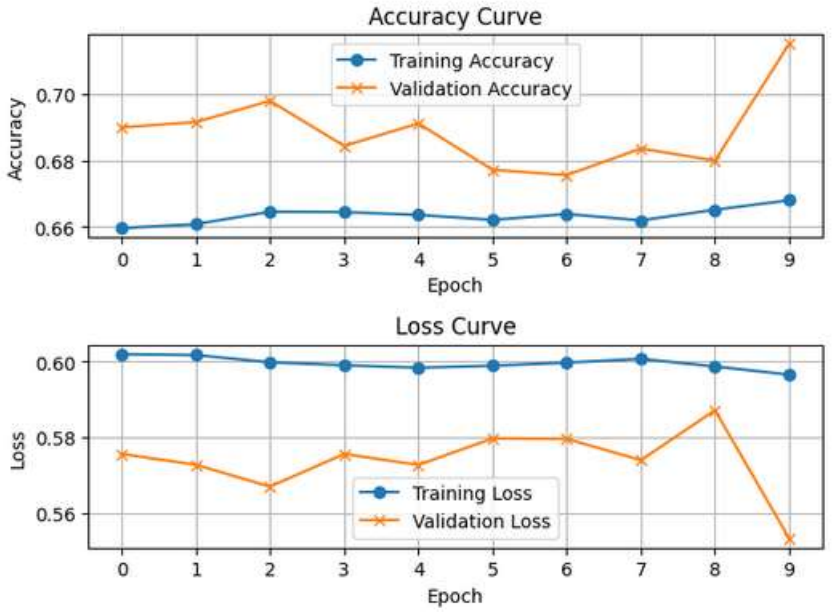

Figure 6.3.3.3 accuracy curve and loss curve of QCNN

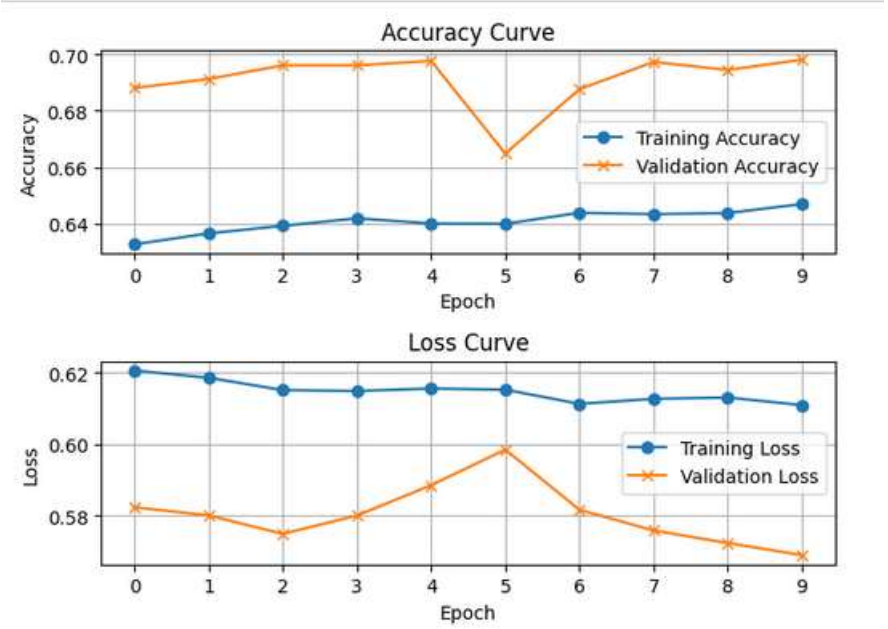

Figure 6.3.3.4 accuracy curve and loss curve of CNN

ROC CURVE

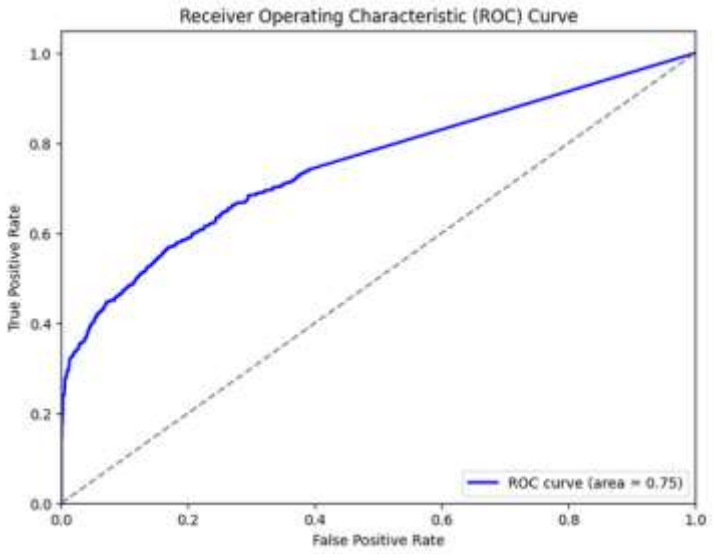

Figure 6.3.3.5 ROC CURVE of QCNN

The QCNN model performs over 0.5 threshold value. The AUC ROC measures the overall performance that is 0.75

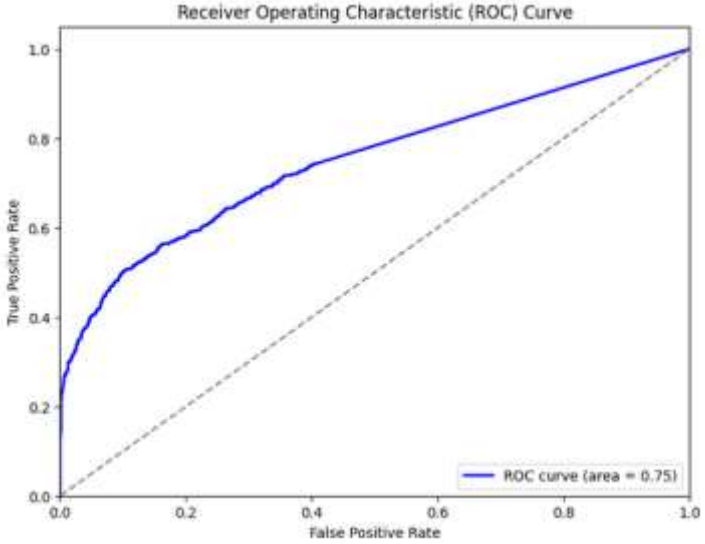

Figure 6.3.3.6 ROC CURVE of CNN

The CNN model performs over 0.5 threshold value. The AUC ROC measures the overall performance that is 0.75

6.3.4 CONCLUSION

In this experiment, we assessed the performance of Convolutional Neural Networks (CNN) and Quantum Convolutional Neural Networks (QCNN) under various noise conditions, specifically with the addition of thermal noise and subsequent noise removal using Wiener filters and Bayesian inference. When thermal noise was added, the QCNN model achieved an AUC ROC of 0.75, correctly predicting 1054 true positives and 647 true negatives, with 199 false positives and 600 false negatives. The CNN model, under the same conditions, had an AUC ROC of 0.74, correctly predicting 984 true positives and 721 true negatives, with 266 false positives and 526 false negatives. These results highlight the challenges both models faced with thermal noise, particularly in terms of increased false positives and false negatives.

Applying Wiener filters to remove thermal noise improved the performance of both models. The QCNN model's AUC ROC increased to 0.76, correctly predicting 1027 true positives and 693 true negatives, with 226 false positives and 554 false negatives. Conversely, the CNN model's AUC ROC decreased to 0.68, correctly predicting 1236 true positives and 354 true negatives, but with a significant number of false negatives (893) despite having only 17 false positives. Bayesian inference provided the most effective noise mitigation, with both models achieving an AUC ROC of 0.75. The QCNN model correctly predicted 1059 true positives and 681 true negatives, with 194 false positives and 566 false negatives. The CNN model correctly predicted 997 true positives and 736 true negatives, with 256 false positives and 511 false negatives. Overall, these findings underscore the importance of advanced noise reduction techniques, with Bayesian inference proving particularly effective in maintaining model accuracy and robustness in the presence of thermal noise.

CHAPTER 7
EXPERIMENTAL RESULT

7.1 COMPARISON BEFORE AND AFTER ADDING NOISE

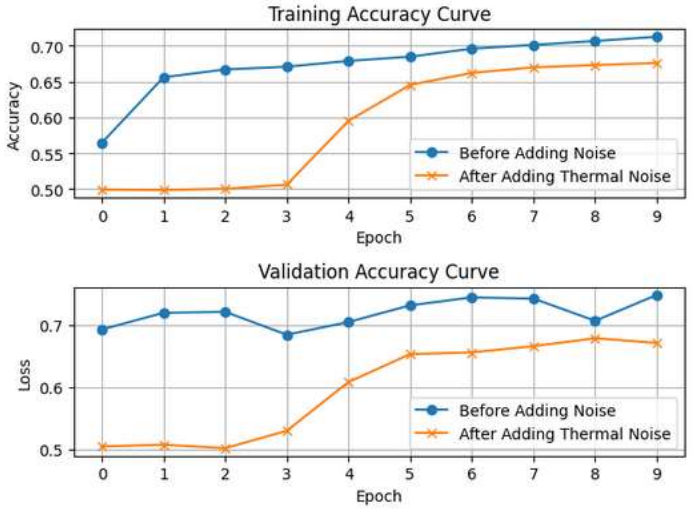

Figure 7.1.1 Training and validation of CNN before and after adding noise

The graph shows less accuracy after adding thermal noise when compared to before adding noise in CNN

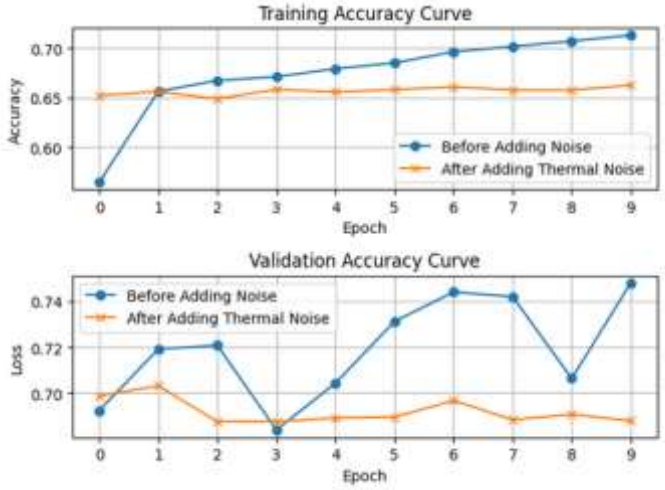

Figure 7.1.2 Training and validation of QCNN before and after adding noise

The graph shows less accuracy after adding thermal noise when compared to before adding noise in QCNN

7.2 COMPARISON AFTER ADDING NOISE AND REMOVING NOISE

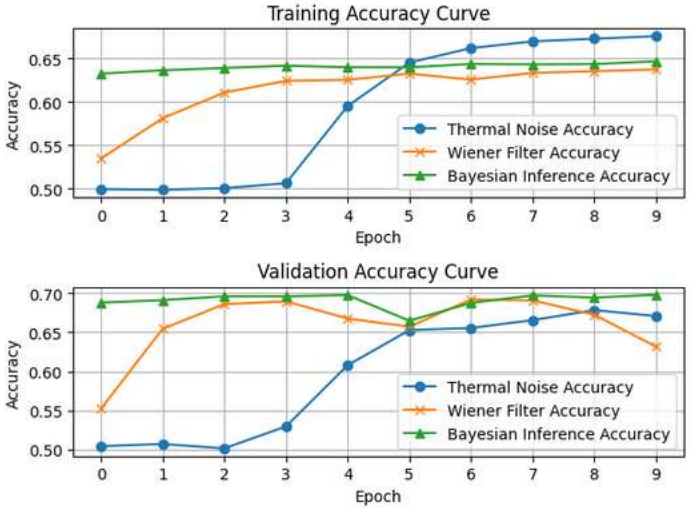

Figure 7.2.1 training and validation of CNN after and removal of noise

The graph shows Bayesian inference method detect better in classification when compared to wiener filter in CNN

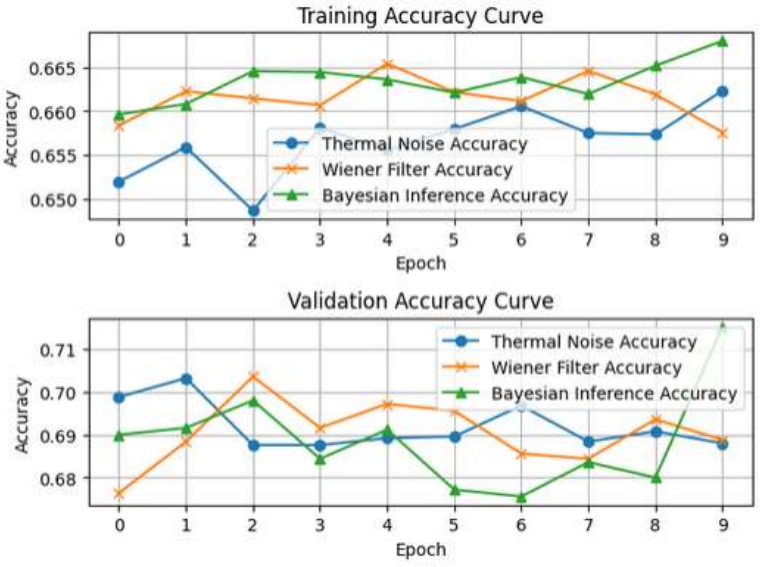

Figure 7.2.1 training and validation of QCNN after and removal of noise

The graph shows Bayesian inference method detect better in classification when compared to wiener filter in QCNN

CHAPTER 8

CONCLUSION

In this project, we explored the application of Quantum Convolutional Neural Networks (QCNNs) for the classification of gravitational wave signals, achieving notable success. QCNNs demonstrated their efficacy in handling large and intricate datasets with remarkable efficiency, surpassing classical algorithms in terms of feature extraction and signal classification. Their ability to discern subtle patterns within the data enabled more accurate identification of gravitational wave signals amidst background noise. Moreover, QCNNs exhibited faster convergence rates compared to traditional methods, highlighting their potential for accelerating data processing in this field

In this study, we introduced controlled thermal noise into the dataset and successfully mitigated it using both the Wiener Filter and Bayesian inference methods. While both approaches significantly improved the signal-to-noise ratio, Bayesian inference emerged as particularly effective in noise detection compared to the Wiener Filter. Its probabilistic approach not only refined the noise removal process but also provided enhanced sensitivity in identifying and distinguishing noise patterns from genuine signals. This underscores Bayesian inference as a pivotal tool in advancing noise reduction techniques, offering greater precision and reliability in scientific data analysis.

This project underscores the promising frontier of Quantum Machine Learning (QML) in advancing gravitational wave astronomy and astrophysics. By integrating QML techniques like QCNNs, we have demonstrated how these methods can push the boundaries of current technological capabilities. They offer avenues for more precise, efficient, and robust analysis of gravitational wave signals, thereby contributing to the broader scientific understanding of the universe's most profound phenomena. As we continue to refine and expand these quantum-inspired approaches, we anticipate further transformative impacts on the field.

REFERENCES

[1] A. Einstein, Sitzungsber. K. Preuss. Akad. Wiss. 1, 688 (1916).

[2] A. Einstein, Sitzungsber. K. Preuss. Akad. Wiss. 1, 154 (1918).

[3] P. R. Saulson, Gen. Relativ. Gravit. 43, 3289 (2011).

[4] K. Schwarzschild, Sitzungsber. K. Preuss. Akad. Wiss. 1, 189 (1916).

[5] D. Finkelstein, Phys. Rev. 110, 965 (1958).

[6] M. D. Kruskal, Phys. Rev. 119, 1743 (1960).

[7] R. P. Kerr, Phys. Rev. Lett. 11, 237 (1963).

[8] C. V. Vishveshwara, Nature (London) 227, 936 (1970).

[9] W. H. Press, Astrophys. J. 170, L105 (1971).

[10] S. Chandrasekhar and S. L. Detweiler, Proc. R. Soc. A 344, 441 (1975).

[11] L. Blanchet, T. Damour, B. R. Iyer, C. M. Will, and A. G. Wiseman, Phys. Rev. Lett. 74, 3515 (1995).

[12] L. Blanchet, Living Rev. Relativity 17, 2 (2014).

[13] A. Buonanno and T. Damour, Phys. Rev. D 59, 084006 (1999).

[14] F. Pretorius, Phys. Rev. Lett. 95, 121101 (2005).

[15] M. Campanelli, C. O. Lousto, P. Marronetti, and Y. Zlochower, Phys. Rev. Lett. 96, 111101 (2006).

[16] J. G. Baker, J. Centrella, D.-I. Choi, M. Koppitz, and J. van Meter, Phys. Rev. Lett. 96, 111102 (2006).

[17] B. L. Webster and P. Murdin, Nature (London) 235, 37 (1972).

[18] C. T. Bolton, Nature (London) 240, 124 (1972).

[19] J. Casares and P. G. Jonker, Space Sci. Rev. 183, 223 (2014).

[20] Badaracco, Francesca, et al. "Machine learning for gravitational-wave detection: surrogate Wiener filtering for the prediction and optimized cancellation of Newtonian noise at Virgo." *Classical and Quantum Gravity* 37.19 (2020): 195016.

[21] Krastev, Plamen G., et al. "Detection and parameter estimation of gravitational waves from binary neutron-star mergers in real LIGO data using deep learning." *Physics Letters B* 815 (2021): 136161.

[22] Zhang, Dingyun. "Detecting gravitational waves using constant-Q transform and convolutional neural networks." *Proceedings of the 2021 4th International Conference on Computational Intelligence and Intelligent Systems*, 2021.

[23] Krastev, Plamen G. "Translating neutron star observations to nuclear symmetry energy via deep neural networks." *Galaxies* 10.1 (2022): 16.

[24] Duraisamy, Premkumar, et al. "Optimized Detection of Continuous Gravitational-Wave Signals using Convolutional Neural Network." *2023 3rd International conference on Artificial Intelligence and Signal Processing (AISP)*. IEEE, 2023.

[25] Krastev, Plamen G. "A deep learning approach to extracting nuclear matter properties from neutron star observations." Symmetry 15.5 (2023): 1123.

[26] Herrmann, Judith, et al. "Detecting Continuous Gravitational Waves Using Generated Training Data." ICASSP 2024-2024 IEEE International Conference on Acoustics, Speech and Signal Processing (ICASSP). IEEE, 2024

[27] M. Burgay et al., "An increased estimate of the merger rate of double neutron stars from observations of a highly relativistic system," *Nature* **426**, 531 (2003).

[28] A.G. Lyne et al., "A double-pulsar system: a rare laboratory for relativistic gravity and plasma physics," *Science* **303**, 1153 (2004).

[29] J. Antoniadis et al., "A massive pulsar in a compact relativistic binary," *Science* **340**, 6131 (2013).

[30] Planck Collaboration, "Planck 2013 results. XVI. Cosmological parameters," *ArXiv e-prints* arXiv:1303.5062 (2013).

[31]S.D.M. White and M.J. Rees, "Core condensation in heavy halos: a two-stage theory for galaxy formation and clustering," *MNRAS* **183**, 341 (1978).

[32] P. Madau and M.J. Rees, "Massive black holes as population III remnants," *ApJ* **551**, L27 (2001).

[33]M.C. Begelman et al., "Formation of supermassive black holes by direct collapse in pre-galactic haloes," *MNRAS* **370**, 289 (2006).

[34] M.C. Begelman et al., "Massive black hole binaries in active galactic nuclei," *Nature* **287**, 307 (1980).

[35] M. Volonteri et al., "Formation and evolution of massive black holes," *ApJ* **582**, 559 (2003).

[36] L. Ferrarese and D. Merritt, "A Fundamental Relation between Supermassive Black Holes and Their Host Galaxies," *ApJ* **539**, L9 (2000).

[37] K. Gebhardt et al., "A Relationship between Nuclear Black Hole Mass and Galaxy Velocity Dispersion," *ApJ* **539**, L13 (2000).

[38] T. R. Marsh, "Double white dwarfs as progenitors of R Coronae Borealis stars and Type I supernovae," *CQG* **28 (9)**, 094019 (2011).

[39] O. Jennrich et al., "The LISA Pathfinder mission," *ESA/SRE* (2011) 19 (2012).

[40] P. Amaro-Seoane et al., "The Gravitational Universe," *GW Notes* **6**, 4 (2013).
[41] D.J. Mortlock et al., "A luminous quasar at a redshift of z = 7.085," *Nature* **474**, 616 (2011).

[42] R. Barkana and A. Loeb, "In the beginning: The first sources of light and the reionization of the universe," *PhysRep* **349**, 125 (2001).

[43] [43] R. H. Becker et al., "Evidence for reionization at z ~ 6: Detection of a Gunn-Peterson trough in a z = 6.28 quasar," *AJ* **122**, 2850 (2001).

[44] J. I. Cirac, D. P´erez-Garc´ıa, N. Schuch, and F. Verstraete, “Matrixproduct states and projected entangled pair states: Concepts, symme-tries, theorems,” Rev. Modern Phys., vol. 93, 2021, Art. no. 045003..

[45] N. D. Mermin, Quantum Computer Science: An Introduction. Cambridge, U.K.: Cambridge Univ. Press, 2007.

[46] Gravitational wave detection dataset: https://www.kaggle.com/competitions/g2net-gravitational-wave-detection/data